LUNG DEVELOPMENT

Rescuing lung development through embryonic inhibition of histone acetylation

Giangela Stokes[1], Zhuowei Li[1], Nicole Talaba[1], William Genthe[2], Maria B. Brix[2], Betty Pham[1], Mark D. Wienhold[3], Gracia Sandok[2], Rebecca Hernan[4], Julia Wynn[4], Haiyang Tang[5], Diana M. Tabima[6], Allison Rodgers[7], Timothy A. Hacker[7], Naomi C. Chesler[8], Pan Zhang[9], Rabi Murad[9], Jason X. -J. Yuan[10], Yufeng Shen[11], Wendy K. Chung[12], David J. McCulley[1]*

A major barrier to the impact of genomic diagnosis in patients with congenital malformations is the lack of understanding regarding how sequence variants contribute to disease pathogenesis and whether this information could be used to generate patient-specific therapies. Congenital diaphragmatic hernia (CDH) is among the most common and severe of all structural malformations; however, its underlying mechanisms are unclear. We identified loss-of-function sequence variants in the epigenomic regulator gene *SIN3A* in two patients with complex CDH. Tissue-specific deletion of *Sin3a* in mice resulted in defects in diaphragm development, lung hypoplasia, and pulmonary hypertension, the cardinal features of CDH and major causes of CDH-associated mortality. Loss of SIN3A in the lung mesenchyme resulted in reduced cellular differentiation, impaired cell proliferation, and increased DNA damage. Treatment of embryonic *Sin3a* mutant mice with anacardic acid, an inhibitor of histone acetyltransferase, reduced DNA damage, increased cell proliferation and differentiation, improved lung and pulmonary vascular development, and reduced pulmonary hypertension. These findings demonstrate that restoring the balance of histone acetylation can improve lung development in the *Sin3a* mouse model of CDH.

INTRODUCTION

Congenital malformations remain the leading cause of infant mortality in the United States and are a major source of newborn morbidity (*1*). One of the most common and severe anomalies is congenital diaphragmatic hernia (CDH), which occurs in 1 of every 3000 to 3500 live births with a mortality rate of 10 to 50% (*2*–*7*). Although abnormal diaphragm development is the hallmark of the disease, the high rate of morbidity and mortality in patients with CDH is due to defects in lung and pulmonary vascular development causing lung hypoplasia and pulmonary hypertension (*8*, *9*). Despite the frequency and severity of CDH, the underlying developmental mechanisms are unclear. Genetic studies in patients and families have identified a growing list of CDH candidate genes implicated in development of the diaphragm (*10*–*13*). Loss-of-function studies of these genes in animal models have demonstrated impaired diaphragm development and a direct role for genetic mutations in the mechanisms responsible for lung hypoplasia and pulmonary hypertension (*14*–*19*).

Epigenetic regulation of gene expression plays an important role throughout development and in physiological adaptation to birth (*20*–*24*). Defects in epigenetic regulation of gene expression have been implicated in the mechanisms responsible for human disease including neurodevelopmental disorders and structural malformations such as congenital heart disease and neural tube defects (*22*, *25*–*30*). Global disruption of DNA methylation or histone acetylation, two of the most well-studied epigenetic mechanisms of gene regulation, results in early embryonic lethality (*31*–*34*). In the lungs, regulation of histone acetylation has been shown to be important for development and in the mechanisms responsible for asthma, chronic obstructive pulmonary disease, pulmonary fibrosis, lung cancer, and pulmonary hypertension (*35*–*43*). The balance of gene transcription and repression maintained by histone acetylation is controlled by the complementary activity of histone acetyltransferase (HAT) and histone deacetylase (HDAC) enzymes (*43*–*45*). The tightly coordinated activity of these enzymes is necessary for rapid changes in gene expression that occur during development and in disease (*46*–*49*).

To direct the timing-, cell-, and genome region–specific action of histone deacetylases, HDAC1 and HDAC2 form multiprotein complexes (*50*–*52*). The Switch-insensitive 3 transcription regulator-histone deacetylase (SIN3)–HDAC complex is one of several such complexes that regulate histone acetylation (*53*–*58*). The SIN3-HDAC complex is most well-known for its role in transcriptional repression by HDAC and regulation of cell cycling during development (*54*–*60*). In addition to its central role in the SIN3-HDAC complex, SIN3 transcription regulator family member A (SIN3A) also activates transcription and has become recognized as a transcriptional coregulator whose function depends on interactions with a wide range of DNA binding cofactors (*59*, *61*–*67*). During development, SIN3A plays multiple roles in organogenesis and cell lineage specification, whereas loss of SIN3A causes defects in energy metabolism and impaired cell cycling (*68*–*74*). Relevant to CDH,

[1]Department of Pediatrics, University of California, San Diego, San Diego, CA 92093, USA. [2]Department of Pediatrics, University of Wisconsin-Madison, Madison, WI 53705, USA. [3]490 BioTech Inc., Knoxville, TN 37996, USA. [4]Department of Pediatrics, Columbia University Irving Medical Center, New York, NY 10032, USA. [5]State Key Laboratory of Respiratory Disease, National Clinical Research Center for Respiratory Disease, Guangzhou Institute of Respiratory Health, First Affiliated Hospital of Guangzhou Medical University, Guangzhou 510120, Guangdong, China. [6]Department of Biomedical Engineering, University of Wisconsin-Madison, Madison, WI 53706, USA. [7]Department of Medicine, University of Wisconsin-Madison, Madison, WI 53705, USA. [8]Edwards Lifesciences Foundation Cardiovascular Innovation and Research Center and Department of Biomedical Engineering, University of California, Irvine, Irvine, CA 92697, USA. [9]Sanford Burnham Prebys Medical Discovery Institute, La Jolla, CA 92037, USA. [10]Section of Physiology, Division of Pulmonary, Critical Care and Sleep Medicine, Department of Medicine, University of California, San Diego, La Jolla, CA 92093, USA. [11]Department of Systems Biology, Department of Biomedical Informatics, and JP Sulzberger Columbia Genome Center, Columbia University Irving Medical Center, New York, NY 10032, USA. [12]Department of Pediatrics, Boston Children's Hospital, Harvard Medical School, Boston, MA 02115, USA.
*Corresponding author. Email: dmcculley@health.ucsd.edu

SIN3A was demonstrated to play a role in skeletal muscle cell development, maintenance, and function (*75*). In the developing lungs, loss of SIN3A in foregut endoderm–derived epithelium resulted in failure of branching morphogenesis and cell cycle arrest (*76*). In adult mice, conditional deletion of *Sin3a* in type 2 alveolar epithelial cells resulted in p53-dependent senescence and pulmonary fibrosis (*77*). Haploinsufficiency or sequence variants in the *SIN3A* gene have been reported in human patients with Witteveen-Kolk syndrome (OMIM 613406), leading to characteristic neurocognitive impairment, growth and feeding difficulties, and distinctive facial features (*78*–*83*). Despite the importance of SIN3A during development, to our knowledge, there are no previous reports of *SIN3A* sequence variants in patients with congenital malformations.

To understand the genetic and developmental mechanisms responsible for CDH, we conducted whole-genome sequencing in patients and family members with the disease. Small deletions that resulted in heterozygous loss of function of *SIN3A* were identified in two patients with complex CDH. To determine the role that SIN3A plays in the development of the diaphragm and lung mesenchyme, we conducted tissue-specific deletion of *Sin3a* in mice. We found that SIN3A is required in the skeletal muscle and mesothelium for diaphragm formation. Furthermore, in the lung mesenchyme, SIN3A is required for cellular differentiation, cell cycling, and regulation of DNA damage. Although SIN3A controls gene expression through multiple mechanisms, we found that loss of SIN3A resulted in an imbalance of histone acetylation and deacetylation, which was restored by embryonic inhibition of HAT.

RESULTS

SIN3A loss-of-function sequence variants were identified in patients with CDH

To identify genetic mechanisms responsible for CDH, whole-genome or -exome sequencing was conducted on 827 patient and parent trios enrolled in the Diaphragmatic Hernia Research and Exploration; Advancing Molecular Science (DHREAMS) study (*13*, *84*). Similar to the epidemiological data reported previously for patients with CDH (*2*–*4*), 59% of this cohort was male, and 33.5% had complex CDH with additional anomalies including congenital heart disease, neurodevelopmental disorders, skeletal anomalies, genitourinary anomalies, and gastrointestinal anomalies (*13*). Among the 1153 protein-coding variants identified were 418 gene damaging variants found in 318 patients with CDH (38.4%) (*13*) including de novo, two– and seven–base pair frameshift deletions in the *SIN3A* gene in two patients with complex CDH (Fig. 1, A and B). The first patient had a two–base pair deletion and frameshift variant in exon 18 and died during the newborn period with a severe, multisystem phenotype including right-sided CDH, respiratory failure, coarctation of the aorta, imperforate anus, and limb abnormalities (Fig. 1B and table S1). The second patient had a seven–base pair deletion and frameshift variant in exon 11 and also exhibited a multisystem phenotype with left-sided CDH, unilateral pelvic kidney, and a palate defect but less severe lung and pulmonary vascular disease and developed schizoaffective disorder (Fig. 1B and table S1). Although growth and neurodevelopmental disorders have been described in patients with *SIN3A* gene variants and Witteveen-Kolk syndrome (*80*, *83*), CDH has not previously been identified in patients with damaging *SIN3A* sequence variants.

To determine whether disruption of SIN3A function might lead to CDH phenotypes, including diaphragm malformation, pulmonary hypertension, or lung hypoplasia, expression of *Sin3a* was characterized in mice. *Sin3a* expression was identified in the developing diaphragm and throughout the lungs at embryonic day 12 (E12, Fig. 1, C to E). In addition to its reported expression in the endoderm-derived epithelium (Fig. 1G) (*76*), *Sin3a* was expressed throughout the developing lung mesenchyme during embryonic and early postnatal stages (Fig. 1, F to H, and fig. S1, A to E) including in *Platelet-derived growth factor receptor alpha* (*Pdgfrα*)–expressing myofibroblasts, *Perilipin 2* (*Plin2*)–expressing lipofibroblasts, *Transgelin* (*Sm22α*)–expressing airway and vascular smooth muscle cells, and *ETS transcription factor* (*Erg*)–expressing lung endothelial cells (fig. S1, F to I).

SIN3A is required in the skeletal muscle and mesothelium for diaphragm development

To determine whether SIN3A is required for diaphragm formation, conditional deletion of *Sin3a* was conducted using cell-specific *Cre*-recombination in cell populations that compose the diaphragm. To investigate the role of SIN3A in the developing diaphragm fibroblasts, *Prx1-Cre* was used to induce recombination in lateral plate mesoderm–derived fibroblast cells that express *Sin3a* (Fig. 2, A and B). Compared with controls (Fig. 2C and fig. S2, A to E), *Prx1-Cre*; *Sin3a* conditional knockout (CKO) embryos exhibited abnormal limb formation (fig. S2F) but normal diaphragm development with *Transcription factor 4* (*Tcf4*)–expressing fibroblast cells, *Myogenic differentiation 1* (*Myod1*)–expressing skeletal muscle cells, and *WT1 transcription factor* (*Wt1*)–expressing mesothelial cells (Fig. 2D and fig. S2, G to J).

To determine whether SIN3A is required in the skeletal muscle during diaphragm development, *Pax3-Cre* was used to induce recombination in somatic mesoderm-derived skeletal muscle that expresses *Sin3a* (Fig. 2, E and F). Compared with controls (Fig. 2G and fig. S2, A to E), *Pax3-Cre*; *Sin3a* CKO embryos had a thin, membranous, and muscle-less diaphragm in addition to other structural defects including anencephaly (Fig. 2H and fig. S2, K to O). The diaphragms of *Pax3-Cre*; *Sin3a* CKO embryos did not contain *Tcf4*-expressing fibroblast or *Myod1*-expressing skeletal muscle cells and were composed exclusively of *Wt1*-expressing mesothelial cells (fig. S2, M to O).

To determine whether SIN3A is required in diaphragm mesothelial cells, *Tbx4-rtTA*; *Tet-o-Cre* was used to induce recombination in the developing mesothelium that expresses *Sin3a* beginning at E6 (Fig. 2, I and J). Compared with controls (Fig. 2K and fig. S2, A to E), deletion of *Sin3a* using this approach resulted in a left-sided, posterior-lateral defect of the diaphragm with herniation of the stomach, intestine, and liver into the left thorax (Fig. 2L and fig. S2, P and Q). This left posterior-lateral diaphragm defect is seen in most patients with CDH. The remaining diaphragms of *Tbx4-rtTA*; *Tet-o-Cre*; *Sin3a* CKO embryos contained *Tcf4*-expressing fibroblast, *Myod1*-expressing skeletal muscle, and *Wt1*-expressing mesothelial cells (Fig. 2, R to T). At the site where the diaphragm failed to close, there was decreased expression of *Tcf4*, normal expression of *Myod1*, and increased and disorganized expression of *Wt1* (fig. S2, U to W). Together, these data suggested that SIN3A is required in both the somatic mesoderm-derived skeletal muscle and the mesothelium during diaphragm development.

SIN3A is required for development of the lung mesenchyme

To investigate the role of SIN3A during lung development, *Tbx4-rtTA*; *Tet-o-Cre* was used to induce deletion of *Sin3a* beginning at E6 (fig. S3A), resulting in recombination throughout the lung mesenchyme and in the diaphragm (fig. S3B). *Tbx4-rtTA*; *Tet-o-Cre*; *Sin3a* CKO mice were born at the expected Mendelian ratio but died after birth (fig. S3C). Compared with controls (fig. S3D), deletion of *Sin3a* using this approach resulted in left CDH with liver herniation into the thorax (fig. S3E) and lung hypoplasia (fig. S3F). Histological analysis of the embryonic thorax revealed that, compared with controls (fig. S3G), *Tbx4-rtTA*; *Tet-o-Cre*; *Sin3a* CKO mice had left-sided CDH, rightward deviation of the heart, liver herniation, and lung hypoplasia (fig. S3H). To determine whether lung hypoplasia in *Tbx4-rtTA*; *Tet-o-Cre*; *Sin3a* CKO mice occurred independent of mechanical compression by herniated abdominal organs, mutant lungs were compared to controls at E12, before organ herniation (fig. S3I). Despite the loss of SIN3A, E12 *Tbx4-rtTA*; *Tet-o-Cre*; *Sin3a* CKO lungs were similar to controls (fig. S3I).

To investigate the role of SIN3A during later stages of lung mesenchymal development without mechanical compression caused by herniated abdominal organs, doxycycline was used to induce recombination throughout the lung mesenchyme beginning at E12 (Fig. 3, A and B). Using this approach, compared with controls that had *Sin3a* expression throughout the lungs (Fig. 3C), *Tbx4-rtTA*; *Tet-o-Cre*; *Sin3a* CKO mice (referred to hereafter as *Sin3a* CKO) lacked expression of *Sin3a* in the mesenchyme but retained expression in the epithelium (Fig. 3D). Despite appearing normal at birth and surviving into adulthood, *Sin3a* CKO mice did not gain weight

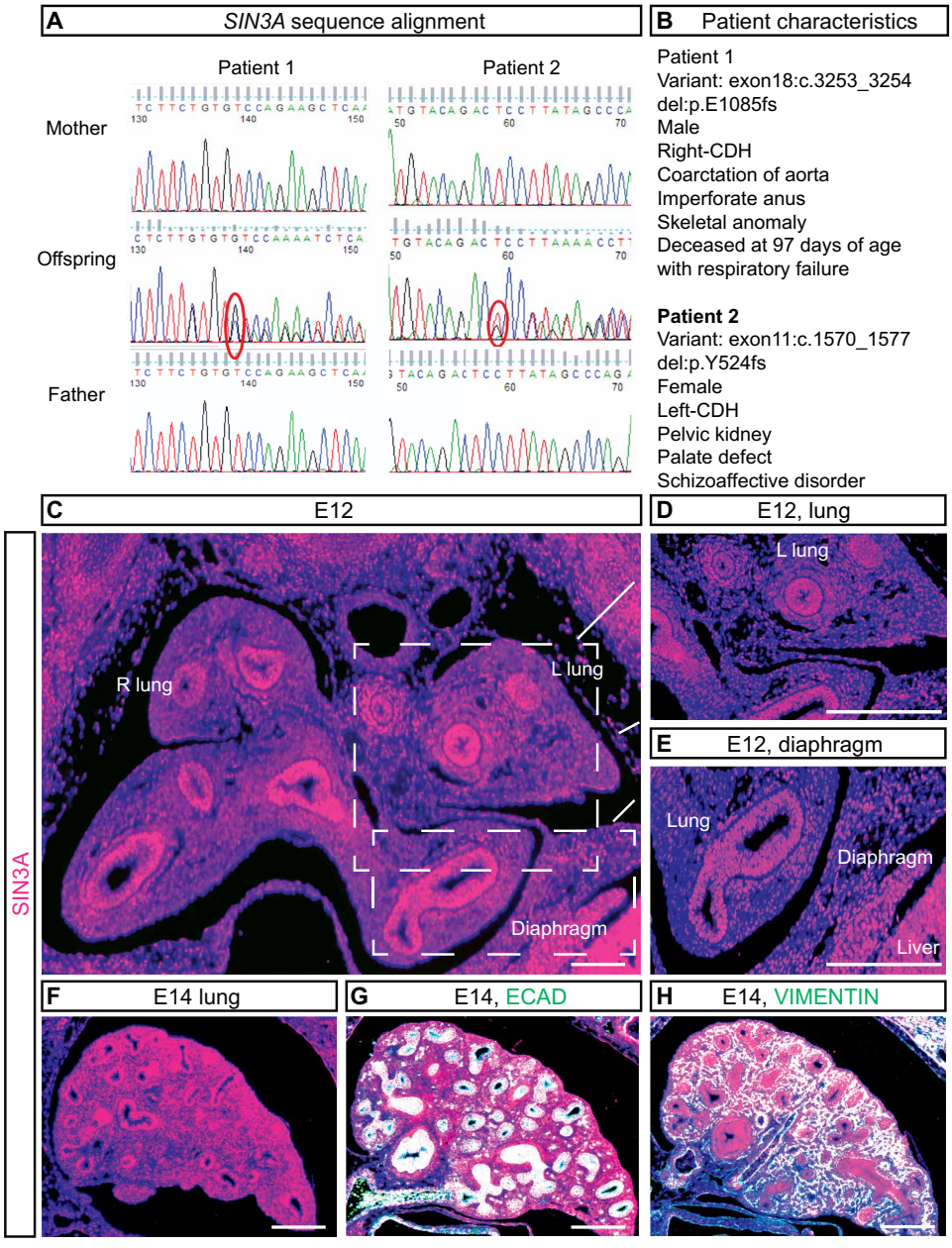

Fig. 1. *SIN3A* sequence variants were present in patients with CDH, and SIN3A is expressed in the developing lungs and diaphragm. (**A**) Sanger sequencing of patient and parent trios identified de novo sequence variants in two patients with complex CDH. (**B**) Characteristics of the patients are provided. (**C** to **E**) Immunofluorescence images of SIN3A (magenta) in the lungs and diaphragms of embryonic mice. (D) and (E) represent higher-magnification images of (C). (**F** to **H**) Immunofluorescence images of SIN3A in embryonic mouse lungs at E14 (F) with E-cadherin (G, ECAD, green) in the epithelium and vimentin (H, VIMENTIN, green) in the mesenchyme (white indicates overlapping immunofluorescence staining). Scale bars, 100 μm.

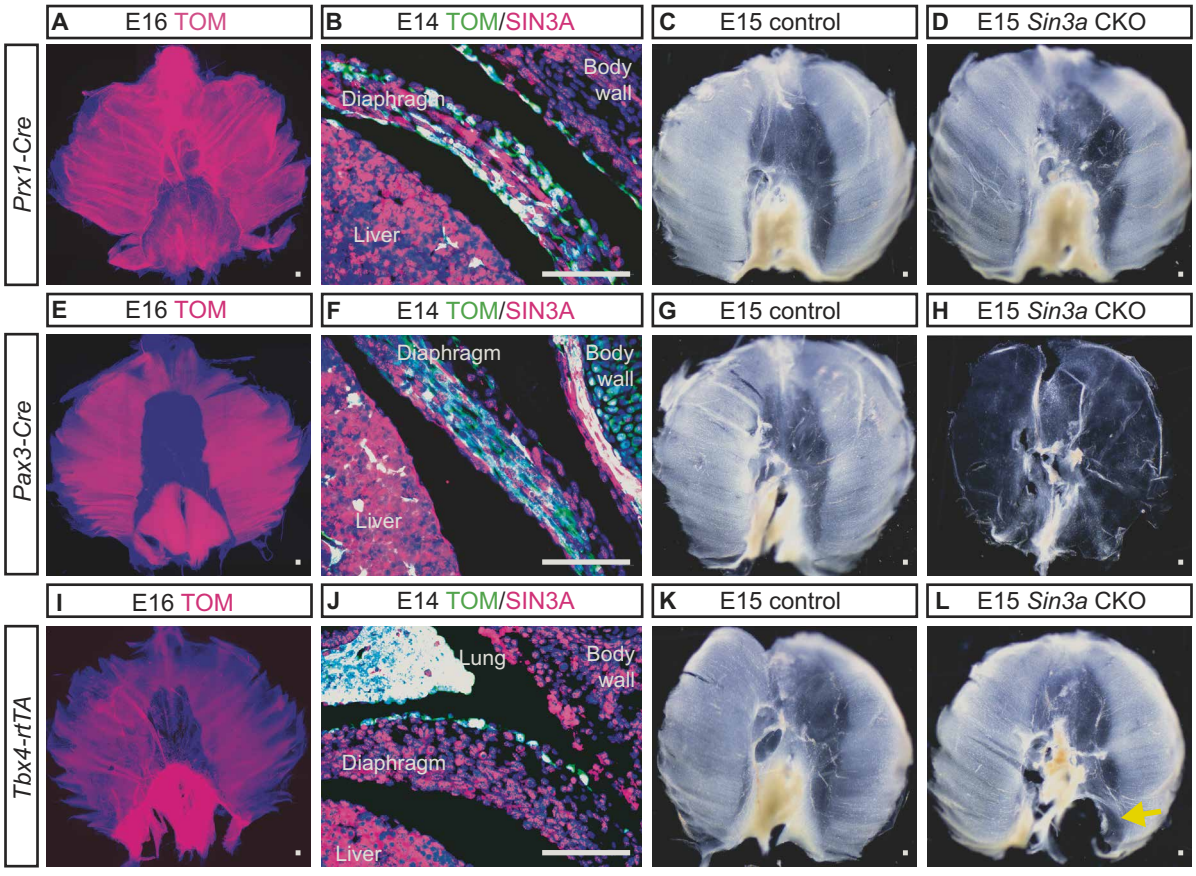

Fig. 2. Conditional deletion of *Sin3a* in the developing mouse diaphragm. (**A** to **D**) *Prx1-Cre* was used to induce recombination in diaphragm fibroblast cells that express *Sin3a*. (A) Whole-mount image of E16 Rosa Tomato fluorescence reporter mouse (Rosa Tomato) diaphragm with *Prx1-Cre*–induced recombination shows recombined Tomato-positive (TOM, magenta) cells throughout the diaphragm. (B) Immunofluorescence image of E14 Rosa Tomato mouse with *Prx1*-Cre–induced recombination shows TOM (magenta) and SIN3A (green; white indicates overlapping immunofluorescence). (C and D) Whole-mount diaphragm images of E15 control (C) and *Prx1-Cre Sin3a* CKO deletion embryos (D). (**E** to **H**) *Pax3-Cre* was used to induce recombination in diaphragm skeletal muscle cells that express *Sin3a*. (E) Whole-mount image of E16 Rosa Tomato mouse diaphragm with *Pax3-Cre*–induced recombination shows recombined TOM-positive cells (magenta). (F) IF image of E14 Rosa tomato with *Pax3-Cre*–induced recombination shows TOM (magenta) and SIN3A (green; white indicates overlapping immunofluorescence). (G and H) Whole-mount diaphragm images of E15 control (G) and *Pax3-Cre Sin3a* CKO embryos (H). (**I** to **L**) *Tbx4-rtTA; Tet-o-Cre* was used to induce recombination in mesothelial cells that expresses *Sin3a*. (I) Whole-mount image of E16 Rosa Tomato mouse diaphragm with *Tbx4-rtTA; Tet-o*–induced recombination shows recombined TOM-positive cells (magenta). (J) IF image of E14 Rosa tomato with *Pax3-Cre*–induced recombination showing TOM (magenta) and SIN3A (green; white indicates overlapping immunofluorescence). (K and L) Whole-mount diaphragm images of E15 control (K) and *Tbx4-rtTA; Tet-o-Cre Sin3a* CKO embryos (L) with defect in the left posterior lateral portion of the diaphragm (L, yellow arrow). Scale bars, 100 μm.

as rapidly as controls (Fig. 3, E and F). Histological analysis at postnatal day 28 (P28) revealed that, compared with controls (Fig. 3G), *Sin3a* CKO mice had emphysematous dilation of the distal airspaces (Fig. 3H). Like newborn patients with CDH, *Sin3a* CKO mice had defects in pulmonary vascular development (Fig. 3, I to L) including decreased lung vessel number and increased vascular smooth muscle wall thickness (Fig. 3, K and L) as well as pulmonary hypertension with right ventricular hypertrophy, increased pulmonary vascular resistance, decreased right ventricular function, and increased right ventricular peak systolic pressure (Fig. 3, M to P). Despite having normal lung size at birth (Fig. 3Q), the first histological evidence of abnormal lung structure was present in *Sin3a* CKO mice at P0 with thickened interstitium and simplified air spaces (Fig. 3, R to T). Pulmonary vascular defects were also present at P0 in *Sin3a* CKO mice with decreased lung vessel number but not vascular smooth muscle hypertrophy (Fig. 3, U to X).

SIN3A is required in the lung mesenchyme for myofibroblast, extracellular matrix, endothelial, and alveolar epithelial cell development

To determine the impact of SIN3A loss of function during lung mesenchymal development, the number and type of lung mesenchymal cells were analyzed in control and *Sin3a* CKO lungs. Compared with controls (Fig. 4A), *Sin3a* CKO lungs had fewer mesenchymal cells (Fig. 4, B and C). Loss of SIN3A resulted in decreased *Pdgfrα*–green fluorescent protein (GFP)–labeled myofibroblast precursor cells, extracellular matrix, and *Elastin* gene expression compared with controls (Fig. 4, D to I). In contrast, lipofibroblast cells were not affected by the loss of SIN3A (Fig. 4, J to L). These data support a primary role for SIN3A in lung mesenchymal cell development in addition to its role in diaphragm formation. Supporting the idea that the mesenchyme plays a central role in directing embryonic lung development, mesenchyme-specific

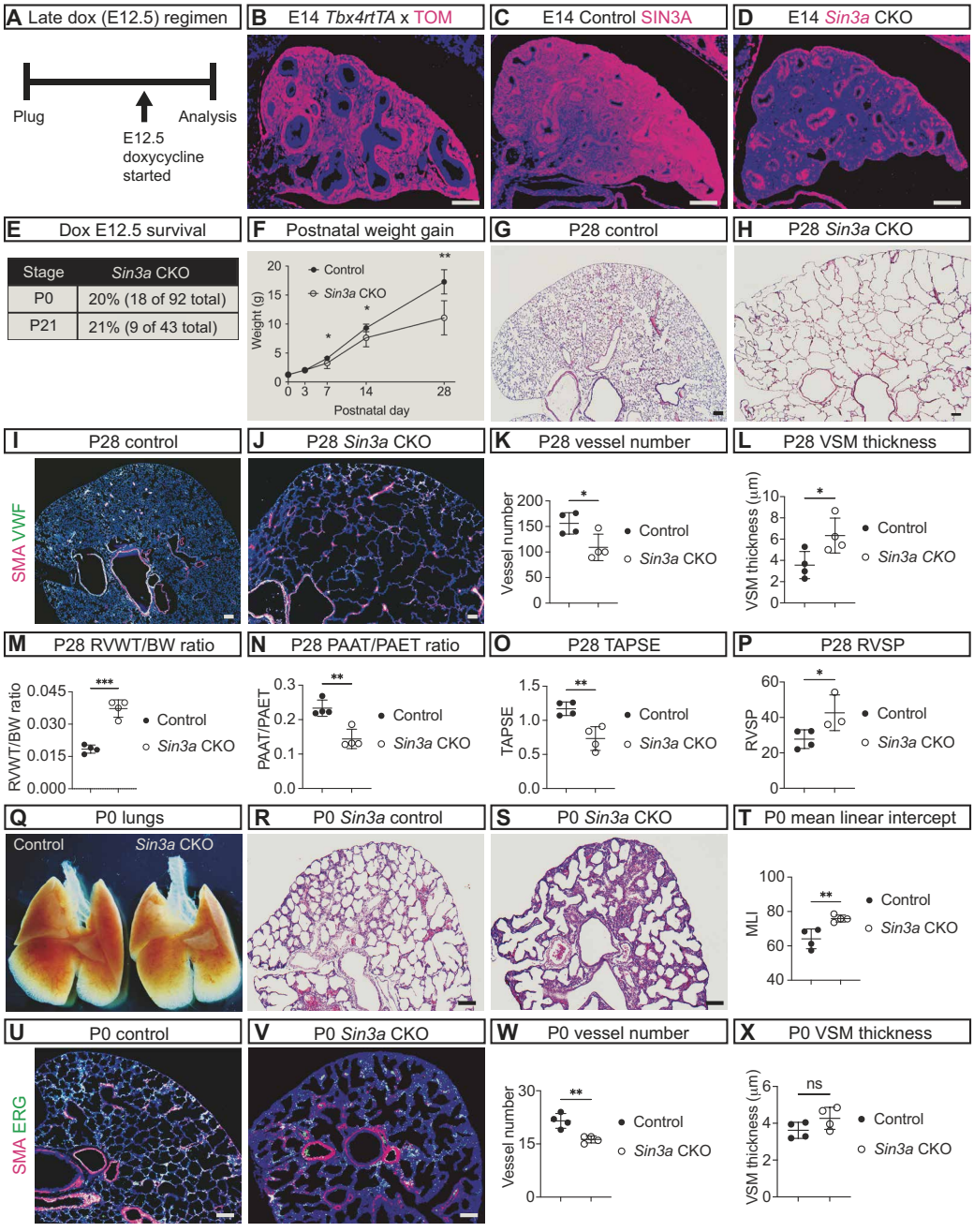

Fig. 3. SIN3A is required in the lung mesenchyme. (**A**) Schematic showing late embryonic (E12) induction of *Tbx4-rtTA; Tet-o-Cre* with doxycycline (Dox). (**B**) Immunofluorescence image of E14 Rosa Tomato mouse lung with late (E12) dox induction of *Tbx4-rtTA; Tet-o-Cre*–mediated recombination shows recombined Tomato-positive cells (TOM, magenta) throughout the lung. (**C** and **D**) Images of SIN3A immunofluorescence (magenta) showing *Sin3a* expression at E14 in control (C) and *Sin3a* CKO lungs (D). (**E**) Percentages of *Sin3a* CKO that survived to P0 and P21. (**F**) Graph depicting weight gain of control and *Sin3a* CKO mice from P0 to P28 (P7 $*P = 0.03$, P14 $*P = 0.04$, P28 $**P = 0.002$). (**G** and **H**) Histological sections of P28 control (G) and *Sin3a* CKO (H) lungs. (**I** to **L**) Immunofluorescence images of von Willebrand factor (VWF, green) for endothelial cells and smooth muscle alpha actin (SMA, magenta) for smooth muscle cells at P28 in control (I) and *Sin3a* CKO (J) lungs with graphs comparing the number of vessels (K, $*P = 0.03$) and width of vascular smooth muscle (L, VSM, $*P = 0.04$). (**M** to **P**) Graphs comparing pulmonary vascular physiology data in P28 control and *Sin3a* CKO mice including echocardiographic measurement of right ventricular hypertrophy (M, RVWT/BW $***P = 0.0008$), pulmonary vascular resistance (N, PAAT/PAET ratio $**P = 0.003$), and right ventricular function (O, TAPSE $**P = 0.008$), with peak systolic right ventricular pressure measured by catheterization of the right ventricular (P, RVSP $*P = 0.04$). (**Q** to **T**) Whole-mount image of P0 lungs from control and *Sin3a* CKO embryos (Q) with histological sections from control (R) and *Sin3a* CKO (S) lungs and graph showing comparison of airspace simplification (T, MLI $**P = 0.008$). (**U** to **X**) Immunofluorescence images of ETS transcription factor (ERG, green) for endothelial cells and smooth muscle (SMA, magenta) from P0 control (U) and *Sin3a* CKO (V) lungs and graphs comparing the number of vessels (W, $**P = 0.004$) and width of smooth muscle (X, $P = 0.13$). RVWT/BW, right ventricle wall thickness to body weight ratio; PAAT/PAET, pulmonary artery acceleration time to pulmonary artery ejection time ratio; TAPSE, tricuspid valve annular plane excursion during systole; RVSP, right ventricle peak systolic pressure; MLI, mean linear intercept. Statistical comparisons of control and *Sin3a* CKO mice were made using unpaired *t* test with statistical significance determined if the *P* value was <0.05. Scale bars, 100 μm.

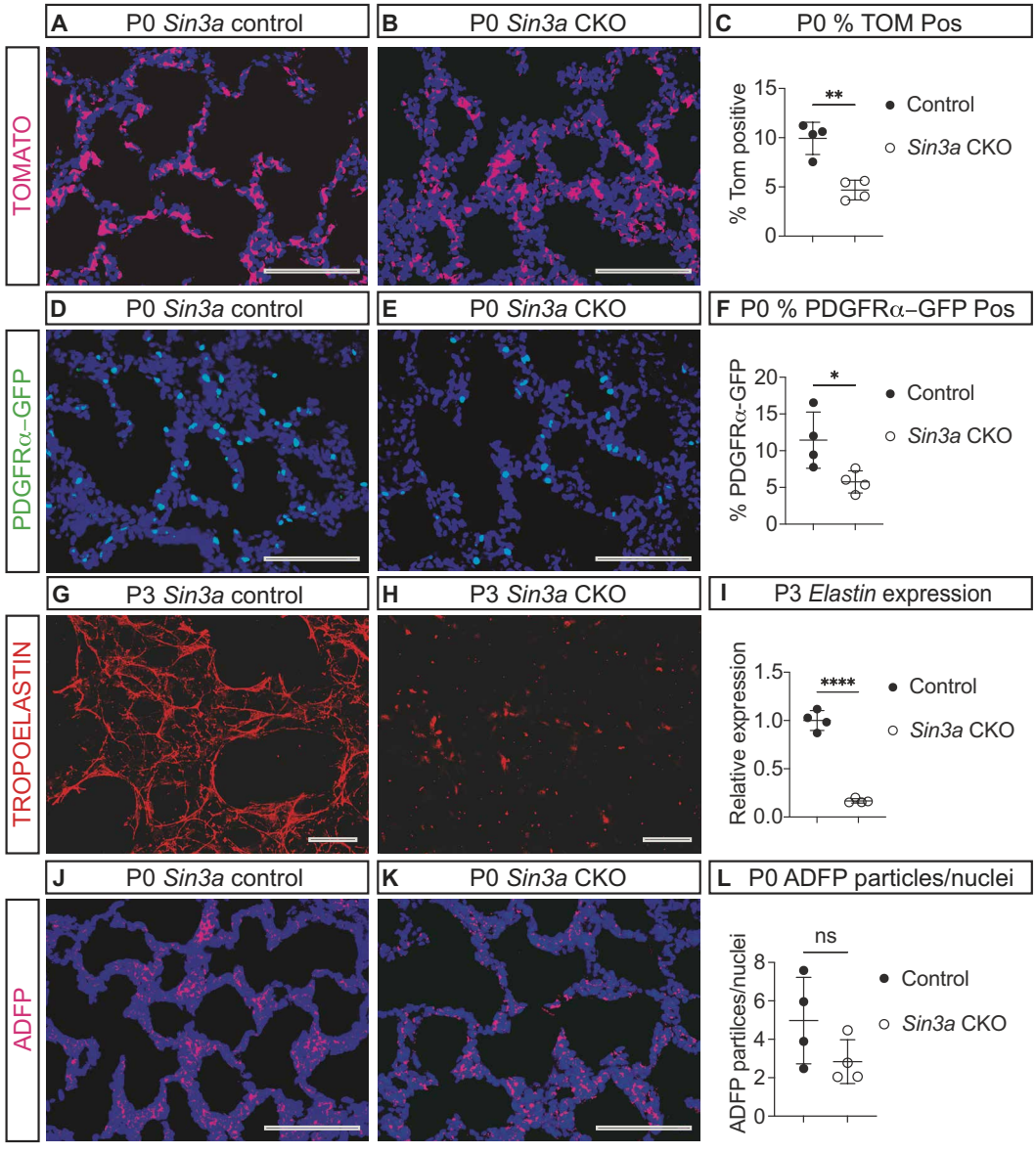

Fig. 4. SIN3A is required in the lung mesenchyme for mesenchymal cell and extracellular matrix development. (**A** and **B**) Images of P0 Rosa Tomato (TOM, magenta) immunofluorescence with (E12) dox induction of *Tbx4-rtTA; Tet-o-Cre*–mediated recombination shows recombined TOM-positive cells (magenta) in P0 control (A) and *Sin3a* CKO (B) mice. (**C**) Graph comparing the percentage of TOM-positive recombined cells in P0 control and *Sin3a* CKO mice (**$P = 0.003$). (**D** and **E**) Images of *Pdgfrα*-GFP (green) immunofluorescence showing myofibroblast precursor cells at P0 in control (D) and *Sin3a* CKO (E) lungs. (**F**) Graph comparing the percentage of *Pdgfrα*-GFP–positive cells (*$P = 0.03$). (**G** and **H**) Images of TROPOELASTIN (red) immunofluorescence in P3 control (G) and *Sin3a* CKO (H) lungs. (**I**) Graph comparing expression of *Elastin* in whole-lung RNA extracts from P3 control and *Sin3a* CKO lungs (****$P < 0.0001$). (**J** and **K**) Images of adipose differentiation–related protein (ADFP, magenta) immunofluorescence in P0 control (J) and *Sin3a* CKO (K) lungs. (**L**) Graph comparing the ratio of ADFP-positive particles per nuclei in P0 control and *Sin3a* CKO lungs ($P = 0.1$). Statistical comparisons between control and *Sin3a* CKO mice were performed using unpaired *t* test with statistical significance determined if the *P* value was <0.05. Scale bars, 100 μm.

deletion of *Sin3a* resulted in decreased *Erg*-expressing alveolar endothelial cells, *Surfactant protein C* (*Sftpc*)–expressing type-2 alveolar epithelial cells, and *Hop homeobox* (*Hopx*)–expressing type-1 alveolar epithelial cells compared with controls (fig. S4, A to I).

To explore the role of SIN3A in vascular development during lung formation, *Cdh5-Cre* was used to delete *Sin3a* in developing endothelial cells (fig. S5A). SIN3A was previously implicated in the transcriptional response of endothelial cells to hypoxia (*85*); however, the role of SIN3A during lung endothelial cell or vascular development has not been demonstrated previously. Compared with controls, *Cdh5-Cre Sin3a* CKO embryos initiated lung development and appeared healthy at E11 (fig. S5, B to E) but developed diffuse hemorrhage between E11 and E12 (fig. S5F), failed to undergo branching morphogenesis (fig. S5, G and H), and experienced disorganized vascular development in the lungs (fig. S5, I to L). These data demonstrated an essential role for SIN3A in endothelial cells for embryonic vascular development.

SIN3A is required for regulation of cell cycling and DNA damage

SIN3A has been demonstrated to direct multiple mechanisms necessary for development, including regulation of cell cycling and cellular differentiation. To determine whether SIN3A plays a similar role in the developing lung mesenchyme, cell proliferation, cell death, and DNA damage were investigated in *Sin3a* CKO mice. Compared to controls, *Sin3a* CKO lungs had a similar number of phosphohistone H3 (PPH3)–positive dividing cells (Fig. 5, A to C) but fewer 5-ethynyl-2 deoxyuridine (EDU)–positive cells undergoing G_1 phase–to–S phase transition (Fig. 5, D to F). In addition, compared with controls, *Sin3a* CKO mice had more cleaved caspase 3 (CC3)–positive cells undergoing apoptosis (Fig. 5, G to I). Last, because loss of SIN3A has been shown to result in increased DNA damage (*86*), immunofluorescence staining for phosphorylated histone variant H2AX at Ser-139 (γH2AX) was used to quantify the number of cells with evidence of DNA damage. Compared with controls, *Sin3a* CKO lungs showed an increase in the number of γH2AX-positive cells (Fig. 5, J to L). These data suggested that loss of SIN3A in the lung mesenchyme resulted in decreased G_1 phase–to–S phase transition, increased programmed cell death, and increased DNA damage.

Loss of SIN3A transcriptional regulation results in impaired lung mesenchymal cell differentiation

To identify the genetic mechanisms responsible for abnormal lung development due to the loss of SIN3A, RNA was collected from the lungs of four control and four *Sin3a* CKO mice at three stages (fig. S6A) including E16, when defects in cell cycling and DNA damage were first evident (Fig. 5, D to F and J to L) and when expression of *Sin3a* was highest (fig. S1A); P0, when the histological phenotype was first evident (Fig. 3, R to T) and when there were changes in the number of mesenchymal, endothelial, and alveolar epithelial cells (Fig. 4, A to F, and fig. S4, A to I); and P3, when there was a reduction in the extracellular matrix (Fig. 4, G to I). Expression of more than 200 genes was altered in *Sin3a* CKO mice at each stage (tables S2 to S4), and 37 genes were misregulated by the loss of SIN3A at all stages (fig. S6A). Consistent with the known role of SIN3A as a transcriptional repressor, deletion of *Sin3a* resulted in increased expression of most of these genes (fig. S6B). Among these

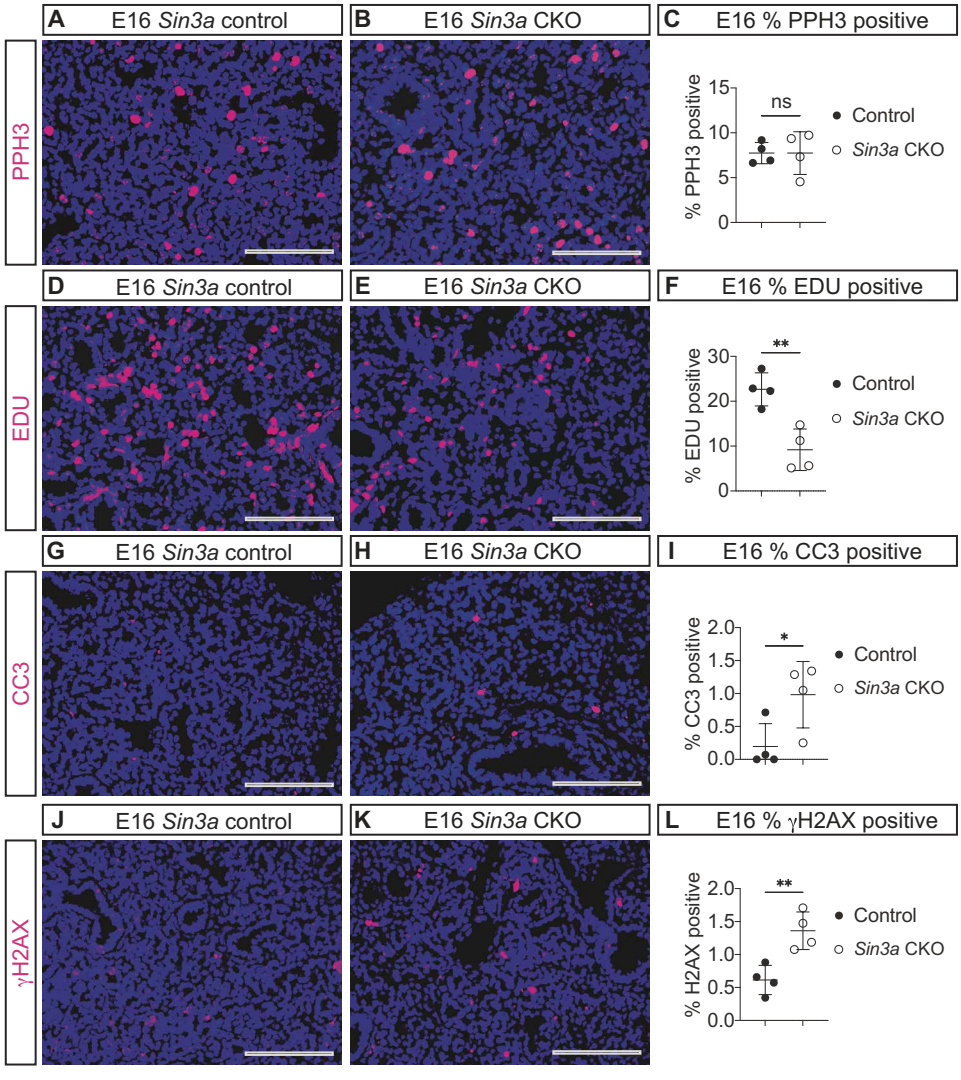

Fig. 5. SIN3A is required for regulation of cell cycling, apoptosis, and DNA damage. (**A** and **B**) Images of phosphohistone H3 (PPH3, magenta) immunofluorescence in E16 control (A) and *Sin3a* CKO (B) lungs. (**C**) Graph comparing the percentage of PPH3-positive cells in E16 control and *Sin3a* CKO lungs ($P = 0.99$). (**D** and **E**) Images of EDU (magenta) immunofluorescence in E16 control (D) and *Sin3a* CKO (E) lungs. (**F**) Graph comparing the percentage of EDU-positive cells in E16 control and *Sin3a* CKO lungs (**$P = 0.004$). (**G** and **H**) Images of cleaved caspase-3 (CC3, magenta) immunofluorescence in E16 control (G) and *Sin3a* CKO (H) lungs. (**I**) Graph comparing the percentage of CC3-positive cells in E16 control and *Sin3a* CKO lungs (*$P = 0.04$). (**J** and **K**) Images of phosphorylated histone H2AX (γH2AX, magenta) immunofluorescence in E16 control (J) and *Sin3a* CKO (K) lungs. (**L**) Graph comparing the percentage of γH2AX-positive cells in E16 control and *Sin3a* CKO lungs (**$P = 0.007$). Statistical comparison of control and *Sin3a* CKO mice was performed using an unpaired *t* test with statistical significance determined if the *P* value was <0.05. Scale bars, 100 μm.

37 genes were those expressed in proliferative lung mesenchymal progenitor cells and that encode regulators of cell cycle progression or G_1 phase–to–S phase transition, including *Ring finger protein 26* (*Rnf26*), *Cytochrome P450 family 26, subfamily A member 1* (*Cyp46a1*), *Cyclin E1* (*Ccne1*), *HECT domain E3 ubiquitin protein ligase 3* (*Hectd3*), *Ribosomal RNA processing 12 homolog* (*Rrp12*), *WD repeat domain 55* (*Wdr55*), and *Transmembrane protein 231* (*Tmem231*) (fig. S6B).

To investigate the changes in gene expression that occurred specifically in lung mesenchymal cells, flow cytometry was used to isolate mesenchymal cells that underwent recombination indicated by the presence of a CRE-responsive red-fluorescence reporter protein from four control and four *Sin3a* CKO mice at E16. Compared with controls, *Sin3a* CKO lung mesenchymal cells had differential expression of more than 4000 genes (Fig. 6A). In contrast to the whole-lung gene expression analysis (fig. S6, A and B), the number of genes with increased expression (2155) was similar to the number with decreased expression (2010) in recombined *Sin3a* CKO mesenchymal cells (Fig. 6A). Among the top 100 misregulated genes were 9 identified in the shared whole-lung gene expression experiment [*Glucosylceramidase beta 1* (*Gba*), *Intraflagellar transport 22* (*Ift22*), *Quinoid dihydropteridine reductase* (*Qdpr*), *Ribonuclease P 40 subunit* (*Rpp40*), *Cyp46a1*, *Ecotropic viral integration site 5 like* (*Evi5l*), *RNA terminal phosphate cyclase-like 1* (*Rcl1*), *Wdr55*, and *KLF transcription factor 16* (*Klf16*)] as well as genes expressed in myofibroblasts [*Desmin* (*Des*)], lipofibroblasts [*Bromodomain adjacent to zinc finger domain 1A* (*Baz1a*)], and extracellular matrix [*Glutathione S-transferase omega 1* (*Gsto1*), *ADAM metallopeptidase with thrombospondin type 1 motif 4* (*Adamts4*), *Cartilage acidic protein 1* (*Crtac1*), *Collagen type IX alpha 2 chain* (*Col9a2*), *Scavenger receptor class A member 3* (*Scara3*), and *Collagen type XVI alpha 1 chain* (*Col16a1*)] (Fig. 6A). Also among the top 100 misregulated genes were those encoding members of the apoptosis pathway [*Superoxide dismutase 2* (*Sod2*), *Inhibitor of growth family member 2* (*Ing2*), *Apoptosis enhancing nuclease* (*Aen*), and *MAX network transcriptional repressor* (*Mnt*)], involved in DNA repair [*Centrosomal protein 164* (*Cep164*), *Centromere protein X* (*Cenpx*), *Sirtuin 7* (*Sirt7*), and *Chromatin assembly factor 1 subunit B* (*Chaf1b*)], and SIN3-associated proteins [SAPs: *Ing2*, *Inhibitor of growth family member 1* (*Ing1*), and *Sin3 associated polypeptide* (*Sap30*); Fig. 6A].

Because impaired mesenchymal cell development was a predominant phenotype observed in the *Sin3a* CKO lungs, we compared the differentially expressed genes with a recently published reference list of genes expressed in mesenchymal cell subpopulations and their precursors (*87*). Compared with controls, *Sin3a* CKO mesenchymal cells had decreased expression of myofibroblast, matrix fibroblast, and lipofibroblast genes (Fig. 6B). By contrast, expression of proliferative progenitor genes was increased in *Sin3a* CKO mesenchymal cells (Fig. 6B). These data were confirmed by quantitative reverse transcription polymerase chain reaction (qRT-PCR) conducted using RNA from whole lungs of E16 *Sin3a* CKO and littermate control mice (Fig. 6B) and suggested that loss of SIN3A resulted in impaired lung mesenchymal cell differentiation.

To investigate the impact of *Sin3a* deletion on mesenchymal cell differentiation, recombined lung mesenchymal cells collected from two control and two *Sin3a* CKO embryos were analyzed using single-cell RNA sequencing (scRNA-seq) at E16 (fig. S7). Using this approach, recombined mesenchymal cells were organized into 14 clusters and broadly categorized as proliferative mesenchymal progenitor cells (PMPs), undifferentiated transitional mesenchymal cells, or differentiating mesenchymal precursor cells (Fig. 6C and fig. S8). Comparison of the relative number of cells within each cluster demonstrated that *Sin3a* CKO lung mesenchymal cells had an increase in proliferative progenitor cells and a decrease in differentiating myofibroblast, matrix, and *Early B cell factor 1* (*Ebf1*)–expressing lung fibroblast precursor cells (Fig. 6 D and E; fig. S9; and table S5). The reduction in differentiating mesenchymal precursor cells was most notable in the myofibroblast cells (Fig. 6E, $^{***}P = 7.63 \times 10^{-39}$, and table S5). These results were similar to the histological data (Fig. 4, D to I) and sorted lung mesenchymal gene expression analysis (Fig. 6B) and suggested that defects in lung development in *Sin3a* CKO mice were due to failure of cell differentiation.

SIN3A is required for lung myofibroblast and matrix fibroblast differentiation

Analysis of spliced and unspliced transcripts using RNA velocity in the scRNA-seq data demonstrated the pattern of differentiation from proliferative mesenchymal cells to transitional undifferentiated mesenchymal cells and then to differentiating mesenchymal precursor cells in control and *Sin3a* CKO lung mesenchymal cells (Fig. 6F). To determine how *Sin3a* deletion affected the potential for cell differentiation, we analyzed the rate of differentiation indicated by RNA velocity lengths (*88*) that were reduced in mesenchymal cells collected from *Sin3a* CKO mice compared with controls (Fig. 6, G and H). The decrease in RNA velocity lengths was observed in PMPs, transitional undifferentiated mesenchymal cells, and differentiating mesenchymal precursor cells (Fig. 6H). These data suggest that loss of SIN3A resulted in the decreased differentiation potential of mesenchymal cells at all stages of differentiation.

To determine the genetic mechanisms responsible for reduced mesenchymal cell differentiation, Ingenuity Pathway Analysis (IPA) was used to identify pathways misregulated by the loss of SIN3A (Fig. 7A). Among the most misregulated canonical pathways and biological processes were pathways relevant for lung development and the phenotype observed in *Sin3a* CKO lungs, including idiopathic pulmonary fibrosis, lung formation, vascular development, entry into S phase, fibroblast cell death, and senescence, where SIN3A has been shown to play a role in lung epithelial cells (Fig. 7A) (*77*). The misregulated upstream regulators included several that play an important role in mesenchyme and lung myofibroblast development and differentiation (Fig. 7, A to C), including decreased expression of myofibroblast and matrix fibroblast genes [*Actin alpha 2, smooth muscle, aorta* (*Acta2*); Myosin, heavy polypeptide 11, smooth muscle (*Myh11*); *Tagln*, *Transforming growth factor–beta induced* (*Tgfbi*); *Des*, *Insulin-like growth factor binding protein 5* (*Igfbp5*); *Eln*, *Insulin-like growth factor binding protein 4* (*Igfbp4*); *Jun D proto-oncogene* (*Jund*); and *Matrix metallopeptidase 2* (*Mmp2*); Fig. 7B] and decreased expression of transforming growth factor–β (TGFB) and WNT pathway genes [*FBJ osteosarcoma oncogene* (*Fos*); Jun proto-oncogene (*Jun*); *Collagen*, *type I*, *alpha 1* (*Col1a1*); *Collagen*, *type III*, *alpha 1* (*Col3a1*); *Collagen*, *type IV*, *alpha 1* (*Col4a1*); *Collagen*, *type VI*, *alpha 3* (*Col6a3*); and *Frizzled class receptor 2* (*Fzd2*); Fig. 7C]. These findings were confirmed using the RNA-seq analysis conducted on sorted lung mesenchymal cells (Fig. 6A) and gene expression analysis conducted on whole-lung RNA extracts at E16, which demonstrated a similar reduction in TGFB and wingless (WNT) pathway gene expression in *Sin3a* CKO lungs (Fig. 7C). Together, these data suggested that loss of SIN3A resulted in altered

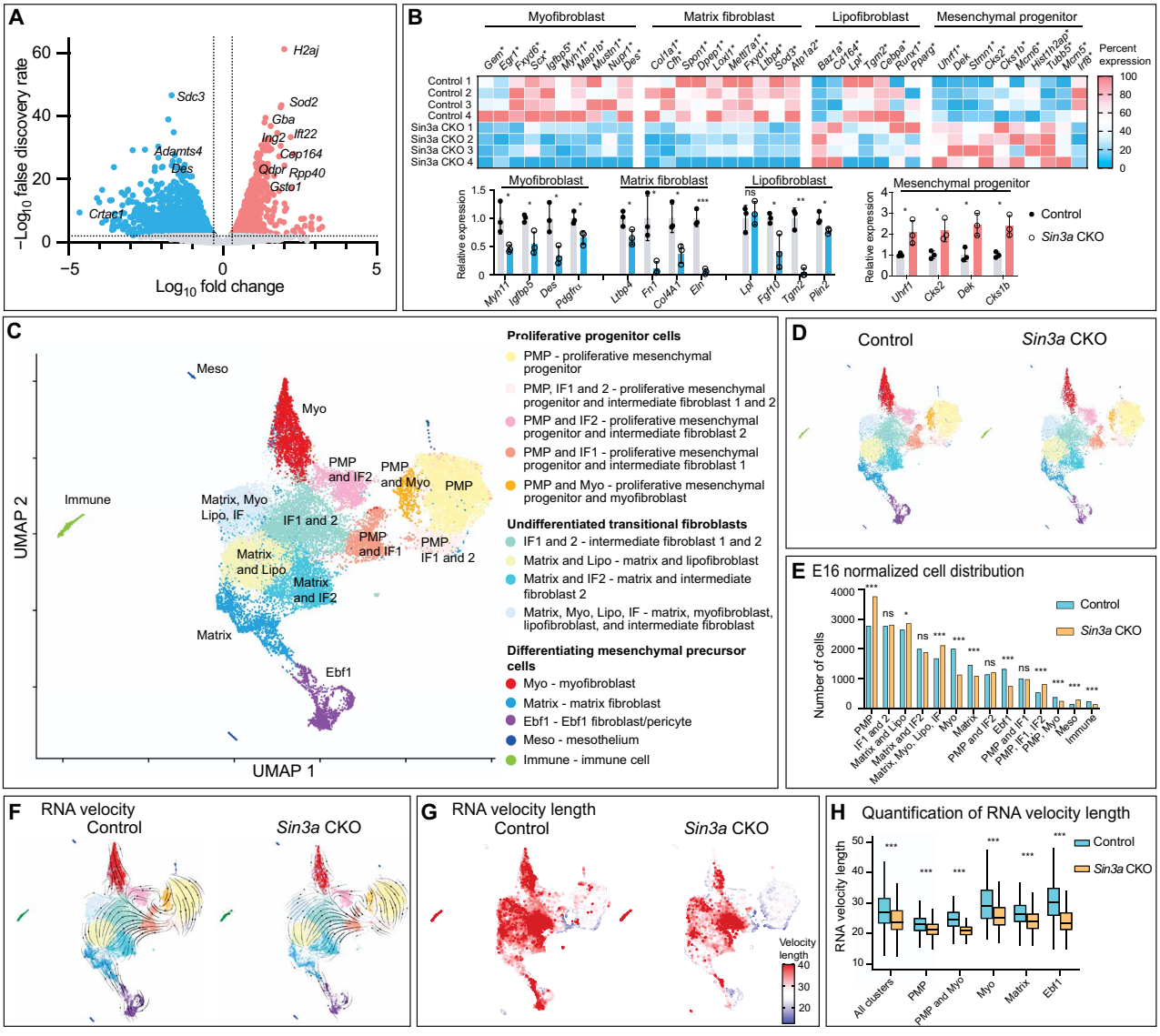

Fig. 6. SIN3A regulates a transcriptional program necessary for mesenchymal cell differentiation. (**A**) Volcano plot of differentially regulated gene expression in recombined lung mesenchymal cells from E16 *Sin3a* CKO compared with controls determined by bulk RNA sequencing [genes with $-\log_{10}$ false discovery rate >2 and $\log_{10}$ fold change >0.301 or <−0.301 (dotted lines) with increased expression are colored red, and those with decreased expression are colored blue]. (**B**) Heatmaps of significantly misregulated individual myofibroblast, matrix fibroblast, lipofibroblast, and mesenchymal proliferative progenitor cell gene expression (*genes with $-\log_{10}$ false discovery rate >2 and $\log_{10}$ fold change >0.301 or <−0.301) in E16 control and *Sin3a* CKO recombined lung cells determined by bulk RNA sequencing and bar graphs of qRT-PCR gene expression performed using whole-lung RNA extracts from E16 control and *Sin3a* CKO embryos showing genes expressed in myofibroblasts (*Myh11*, $^*P = 0.03$; *Igfbp5*, $^*P = 0.02$; *Des*, $^*P = 0.02$; and *Pdgfrα*, $^*P = 0.02$), matrix fibroblasts (*Ltbp4*, $^*P = 0.04$; *Fn1*, $^*P = 0.02$; *Col4a1*, $^*P = 0.02$; and *Eln*, $^{***}P = 0.0005$), lipofibroblasts (*Lpl*, $P = 0.63$; *Fgf10*, $^*P = 0.03$; *Tgm2*, $^{**}P = 0.001$; and *Adfp*, $^*P = 0.03$), and proliferating mesenchymal progenitor cells (*Uhrf1*, $^*P = 0.03$; *Cks2*, $^*P = 0.02$; *Dek*, $^*P = 0.01$; and *Cks1b*, $^*P = 0.01$). Statistical comparisons of gene expression analyzed by qRT-PCR between control and *Sin3a* CKO whole-lung RNA were performed using unpaired *t* test. (**C**) Uniform Manifold Approximation and Projection (UMAP) of clustered recombined E16 lung mesenchymal cells from control and *Sin3a* CKO mice analyzed by scRNA-seq categorized into three groups: proliferative progenitor cells, undifferentiated transitional fibroblasts, and differentiating mesenchymal precursor cells. (**D** and **E**) Comparison of E16 control and *Sin3a* CKO UMAPs (D) and bar graphs comparing the percentage of cells within each cluster in the control and *Sin3a* CKO recombined lung mesenchymal cells (PMP, $^{***}P = 2.67 \times 10^{-26}$; IF1 and IF2, $P = 0.59$; Matrix and Lipo, $^*P = 0.02$; Matrix and IF2, $P = 0.15$; Matrix, Myo, Lipo, and IF, $^{***}P = 6.36 \times 10^{-9}$; Myo, $^{***}P = 7.63 \times 10^{-39}$; Matrix, $^{***}P = 7.43 \times 10^{-10}$; PMP and IF2, $P = 0.20$; Ebf1, $^{***}P = 7.86 \times 10^{-26}$; PMP and IF1, $P = 0.58$; PMP, IF1, and IF2, $^{***}P = 2.18 \times 10^{-10}$; PMP and Myo, $^{***}P = 6.66 \times 10^{-5}$; Meso, $^{***}P = 3.67 \times 10^{-9}$; Immune, $^{***}P = 4.92 \times 10^{-6}$). Statistical comparison of the distribution of cells within each cluster between control and *Sin3a* CKO recombined lung mesenchymal cells was conducted using χ^2 test. (**F** and **G**) UMAPs showing RNA velocity analysis of scRNA-seq data from E16 control and *Sin3a* CKO recombined lung mesenchymal cells (F) and heatmap of RNA velocity lengths (G). (**H**) Box and whisker plot comparing RNA velocity length in E16 control and *Sin3a* CKO recombined lung mesenchymal cell clusters ($^{***}P = 4.72 \times 10^{-281}$), proliferative mesenchymal progenitor cells (PMP, $^{***}P = 8.02 \times 10^{-20}$ and PMP/myofibroblast, $^{***}P = 2.20 \times 10^{-9}$), and differentiating mesenchymal precursor cells (H, myofibroblast, $^{***}P = 2.30 \times 10^{-32}$; matrix fibroblast, $^{***}P = 2.09 \times 10^{-15}$; and Ebf1 fibroblast cells, $^{***}P = 3.51 \times 10^{-46}$). Statistical comparisons of RNA velocity between control and *Sin3a* CKO recombined lung mesenchymal cells analyzed by scRNA-seq were performed using *Z* test.

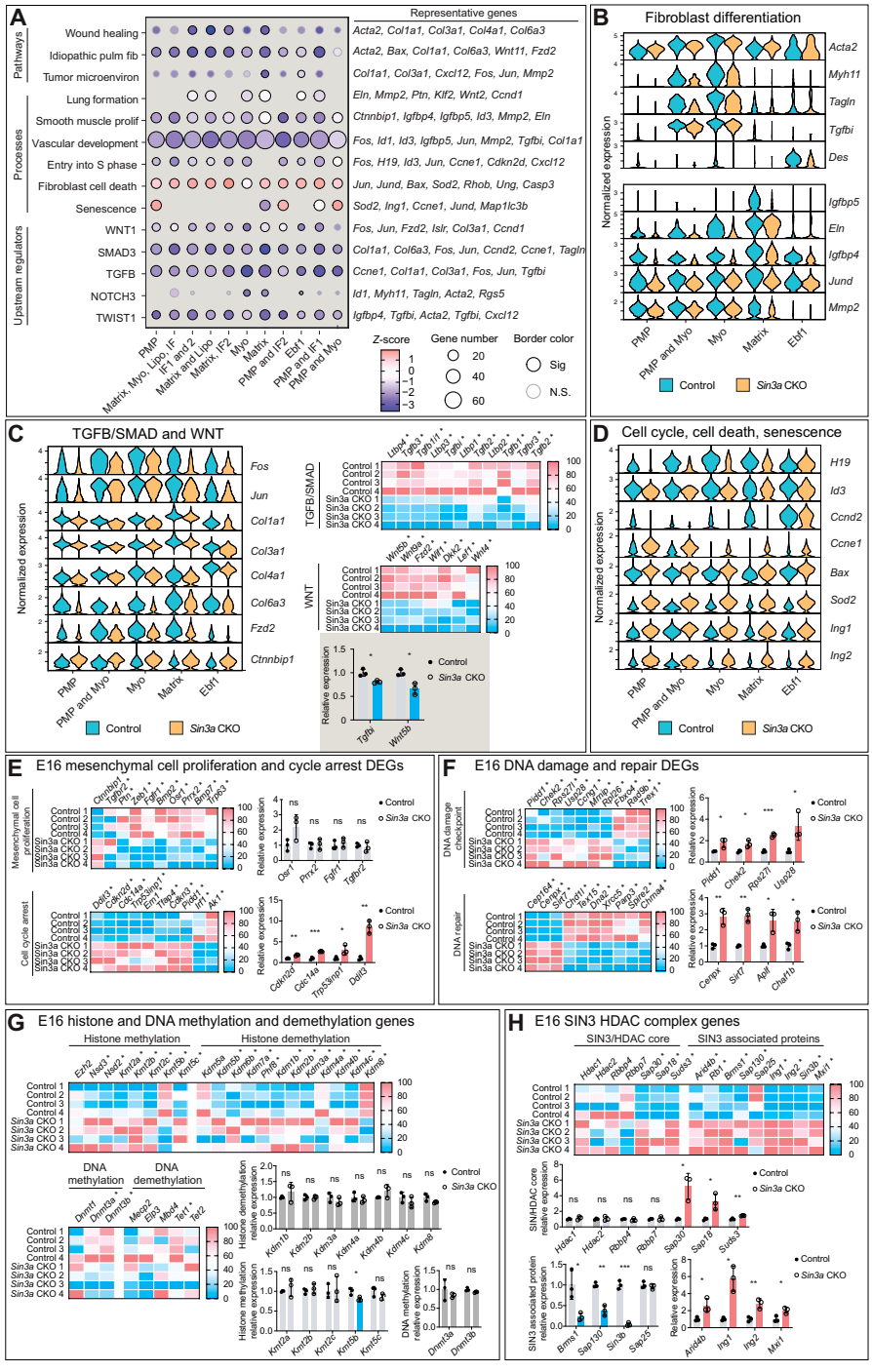

Fig. 7. SIN3A is required for regulation of mesenchymal cell differentiation, cell cycling, DNA damage, and senescence. (**A**) IPA of differential gene expression conducted using scRNA-seq data performed on recombined lung mesenchymal cells from E16 control and *Sin3a* CKO embryos. Shown are data demonstrating misregulation of pathways, processes, and upstream regulators of gene expression and representative differentially regulated genes. (**B**) Violin plots comparing the expression of genes that regulate fibroblast differentiation in E16 control and *Sin3a* CKO recombined lung mesenchymal cells analyzed by scRNA-seq in PMP, PMP and myofibroblast (PMP and Myo), Myo, matrix, and *Ebf1*-expressing fibroblast (Ebf1) cell clusters. (**C**) Violin plots comparing the expression of TGFB/SMAD and WNT pathway genes in E16 control and *Sin3a* CKO recombined lung mesenchymal cells analyzed by scRNA-seq in PMP, PMP and Myo, Myo, Matrix, and Ebf1 cell clusters as well as heatmaps comparing the TGFB/SMAD and WNT pathway genes with significantly different expression (*genes with $-\log_{10}$ false discovery rate >2 and $\log_{10}$ fold change >0.301 or <−0.301) in recombined lung mesenchymal cells from E16 control and *Sin3a* CKO lungs analyzed by bulk RNA sequencing and bar graphs comparing the relative expression of *Tgbi* (*$P = 0.01$) and *Wnt5b* (*$P = 0.01$) determined by qRT-PCR analysis of whole-lung RNA extracts from E16 control and *Sin3a* CKO embryos. (**D**) Violin plots comparing the expression of genes that promote cell cycling (*H19*, *Id3*, and *Ccnd2*) and genes that promote cell death and senescence (*Ccne1*, *Bax*, *Sod2*, and *Ing1*) in E16 control and *Sin3a* CKO recombined lung mesenchymal cells analyzed by scRNA-seq and IPA of PMP, PMP and Myo, Myo, Matrix, and Ebf1 cell clusters. (**E**) Heatmaps comparing the expression of significantly misregulated genes (*genes with – $\log_{10}$ false discovery rate > 2 and $\log_{10}$ fold change >0.301 or <−0.301) that promote cell cycle progression and cell cycle arrest in recombined lung mesenchymal cells from E16 control and *Sin3a* CKO cells analyzed by bulk RNA-seq and bar graphs comparing the relative expression of genes that promote cell cycle progression (*Osr1*, $P = 0.08$; *Prrx2*, $P = 0.78$; *Fgfr1*, $P = 0.52$; *Tgfbr2*, $P = 0.58$) or cell cycle arrest (*Cdkn2d*, **$P = 0.002$; *Cdc14a*, ***$P = 0.0007$; *Trp53inp1*, *$P = 0.04$; *Ddit* **$P = 0.001$) conducted on whole-lung RNA extracts from E16 control and *Sin3a* CKO lungs. (**F**) Heatmaps comparing the expression of significantly misregulated DNA damage checkpoint genes or genes that are expressed during DNA repair (*genes with $-\log_{10}$ false discovery rate >2 and $\log_{10}$ fold change >0.301 or <−0.301) in recombined lung mesenchymal cells from E16 control and *Sin3a* CKO cells analyzed by bulk RNA-seq and bar graphs comparing the relative expression of DNA damage checkpoint genes (*Pidd1*, *$P = 0.03$; *Chek2*, *$P = 0.03$; *Rps27l*, ***$P = 0.0003$; *Usp28*, *$P = 0.04$) or genes expressed during DNA repair (*Cenpx*, **$P = 0.004$; *Sirt7*, **$P = 0.001$; *Aplf*, *$P = 0.02$; *Char1b*, *$P = 0.01$) analyzed by qRT-PCR conducted on whole-lung RNA extracts from E16 control and *Sin3a* CKO lungs. (**G**) Heatmaps comparing the expression of genes that encode histone methyltransferase, histone demethylase, DNA methyltransferase, and DNA demethylase factors (*genes with $-\log_{10}$ false discovery rate >2 and $\log_{10}$ fold change >0.301 or <−0.301) in recombined lung mesenchymal cells from E16 control and *Sin3a* CKO cells analyzed by bulk RNA-seq and bar graphs comparing the relative expression of histone methyltransferase (*Kmt5b*, *$P = 0.03$), histone demethylase, DNA methyltransferase, and DNA demethylase genes analyzed by qRT-PCR conducted on whole-lung RNA extracts from E16 control and *Sin3a* CKO lungs. (**H**) Heatmaps comparing the expression of genes that encode SIN3-HDAC complex core component factors or SAPS (*genes with $-\log_{10}$ false discovery rate >2 and $\log_{10}$ fold change >0.301 or <−0.301) in recombined lung mesenchymal cells from E16 control and *Sin3a* CKO cells analyzed by bulk RNA-seq and bar graphs comparing the relative expression of SIN3-HDAC core complex (*Sap30*, *$P = 0.01$; *Sap18*, *$P = 0.02$; and *Suds3*, **$P = 0.004$) or SAP genes (*Brms1*, *$P = 0.02$, *Sap130*, **$P = 0.001$; *Arid4b*, *$P = 0.03$; *Ing1*, **$P = 0.005$; *Ing2*, **$P = 0.007$; and *Mxi1*, *$P = 0.02$) analyzed by qRT-PCR conducted on whole-lung RNA extracts from E16 control and *Sin3a* CKO lungs. Statistical comparisons of gene expression analyzed by qRT-PCR in control and *Sin3a* CKO whole-lung RNA were performed using unpaired *t* test. Statistical significance was determined if the *P* value was <0.05.

gene expression in pathways required for myofibroblast and matrix fibroblast differentiation.

SIN3A deletion altered gene expression, leading to impaired cell cycling, DNA damage, and senescence

In addition to the changes in mesenchymal cell differentiation, pathway and differential gene expression analysis of *Sin3a* CKO mesenchymal cells demonstrated decreased entry into S phase (Fig. 7A) with decreased expression of genes that promote cell cycle progression [*H19 imprinted maternally expressed transcript* (*H19*), *Inhibitor of DNA binding 3* (*Id3*), and *Cyclin D2* (*Ccnd2*)]; increased expression of genes associated with cell cycle arrest, cell death, or senescence [*Ccne1*, *BCL2-associated X protein* (*Bax*), *Sod2*, and *Ing1*]; and increased expression of *Ing2*, one of the SAPs (Fig. 7D). These findings were confirmed using the sorted lung mesenchymal RNA-seq analysis (Fig. 6A) and gene expression analysis conducted on RNA extracted from E16 control and *Sin3a* CKO lungs (Fig. 7, E to H). Loss of SIN3A resulted in reduced expression of genes that promote mesenchymal cell proliferation and increased expression of genes that promote cell cycle arrest (Fig. 7E). *Sin3a* CKO mice also had increased expression of genes expressed in response to DNA damage and altered expression of genes associated with DNA repair (Fig. 7F). These data supported the conclusion that SIN3A is required during lung development to promote mesenchymal cell differentiation and that loss of SIN3A resulted in impaired cell cycling and increased DNA damage.

Pathway and single-cell gene expression analysis demonstrated that loss of SIN3A resulted in increased expression of genes involved in senescence (Fig. 7, A and D). SIN3A has been demonstrated to regulate genes implicated in senescence, and loss of SIN3A in the lung epithelium was associated with senescence and pulmonary fibrosis (*76*, *77*). Compared with controls, *Sin3a* CKO mesenchymal cells had differential expression of multiple genes associated with senescence (fig. S10, A to C). This expression analysis did not indicate an increase or decrease in senescence activation because genes that promote or repress senescence were both positively and negatively affected by the loss of SIN3A (fig. S10, A to C). These data suggested that loss of SIN3A in the mesenchyme resulted in an accumulation of progenitor cells, decreased cell cycling, increased DNA damage, and senescence.

SIN3A is required for controlling the balance of histone acetylation

SIN3A regulates gene expression during development through multiple mechanisms including histone and DNA methylation and demethylation (*59*, *89*) and was recently demonstrated to play a role in pulmonary hypertension by regulating methylation of the *bone morphogenetic protein receptor type 2* (*BMPR2*) promoter (*90*). Gene expression analysis of sorted lung mesenchymal cells from *Sin3a* CKO and control lungs at E16 demonstrated increased expression of genes that promote both histone methylation and demethylation, whereas genes that promote DNA methylation or demethylation were decreased (Fig. 7G). Gene expression analysis conducted on whole-lung RNA extracts from *Sin3a* CKO and control mice at E16 did not demonstrate a consistent trend in either histone or DNA methylation (Fig. 7G). Because more of the genes that direct histone methylation or demethylation were misregulated in *Sin3a* CKO recombined mesenchymal cells, immunofluorescence staining for transcriptional repressing methylation of histone 3 lysine 9 (H3K9Me2 and H3K9Me3) and lysine 27 (H3K27Me3) was conducted at E16 (fig. S11, A to I). These data demonstrated that no significant change in histone methylation was detectable despite the loss of SIN3A during lung mesenchymal development (fig. S11, A to I; $P = 0.46$ for H3K9Me2, $P = 0.64$ for H3K9Me3, and $P = 0.57$ for H3K27Me3).

SIN3A is known to act as a transcriptional repressor through its cooperative interaction with HDACs. The activity of the SIN3-HDAC complex is modulated by multiple cofactors (*53*, *91*, *92*). In recombined *Sin3a* CKO lung mesenchymal cells at E16 (Fig. 6A), expression of the SIN3-HDAC core complex and SAP genes was upregulated, including *Sap30*, *Sin3-associated polypeptide 18* (*Sap18*), *Suppressor of defective silencing 3 homolog* (*Suds3*), *AT-rich interaction domain 4B* (*Arid4b*), *RB transcriptional corepressor 1* (*Rb1*), *Breast cancer metastasis-suppressor 1* (*Brms1*), *Sin3A-associated protein 130* (*Sap130*), *Sin3-associated polypeptide* (*Sap25*), *Ing1*, *Ing2*, *Transcriptional regulator, SIN3B* (*Sin3b*), and *MAX interactor 1 dimerization protein* (*Mxi1*) (Fig. 7H). These data were confirmed by gene expression analysis conducted on whole-lung RNA extracts from *Sin3a* CKO and control embryos at E16 demonstrating misregulated expression of both core SIN3-HDAC and SAP cofactors (Fig. 7H). By contrast, expression of HAT genes *CREB-binding protein* (*Crebbp*) and *E1A-binding protein p300* (*Ep300*) was not changed in lung mesenchymal cells from *Sin3a* CKO embryos (fig. S12).

To determine whether loss of SIN3A in the lung mesenchyme had a direct impact on the balance of histone acetylation, immunofluorescence staining for transcriptional activating acetylation of H3K9 and H3K27 was conducted on *Sin3a* CKO and control lungs (fig. S13, A to F). These data demonstrated that loss of SIN3A resulted in increased histone acetylation in *Sin3a* CKO lungs (fig. S13, C and F). The imbalance of histone acetylation and deacetylation observed in *Sin3a* CKO lungs might be responsible for the observed changes in gene expression and the decrease in mesenchymal cell differentiation, decrease in cell cycling, and increase in DNA damage.

To investigate this hypothesis and to determine whether embryonic inhibition of HDAC recapitulated SIN3A loss of function, untreated control and *Sin3a* CKO mice (Fig. 8, A to F) were compared to those treated with dimethyl sulfoxide (DMSO) vehicle control (fig. S14, A to F) and to those treated with HDAC inhibitor trichostatin A (TSA) beginning when doxycycline-induced recombination was initiated (Fig. 8G and fig. S14, G to L) (*93*, *94*). Using this approach, there was no difference in the number of EDU-positive cells in untreated *Sin3a* CKO lungs (Fig. 8B) compared to those treated with DMSO vehicle control (fig. S14, B and C) or those treated with TSA (fig. S14, H and I). In contrast, compared with untreated control lungs (Fig. 8A) or those treated with DMSO (fig. S14A), there was a reduction in the number of EDU-positive cells in control lungs treated with TSA (fig. S14, G and I). The number of EDU-positive cells in control lungs treated with TSA was similar to the number of EDU-positive cells in untreated *Sin3a* CKO lungs (Fig. 8B and fig. S14, G and I). These data suggested that embryonic HDAC inhibition with TSA resulted in decreased G_1 phase–to–S phase transition that was similar to loss of SIN3A function. HDAC inhibition with TSA did not alter the number of cells with evidence of DNA damage indicated by γH2AX staining in either *Sin3a* CKO or control lungs (Fig. 8, D to F, and fig. S14, D to F and J to L), suggesting that DNA damage observed in *Sin3a* CKO mice might not be due to decreased HDAC function alone.

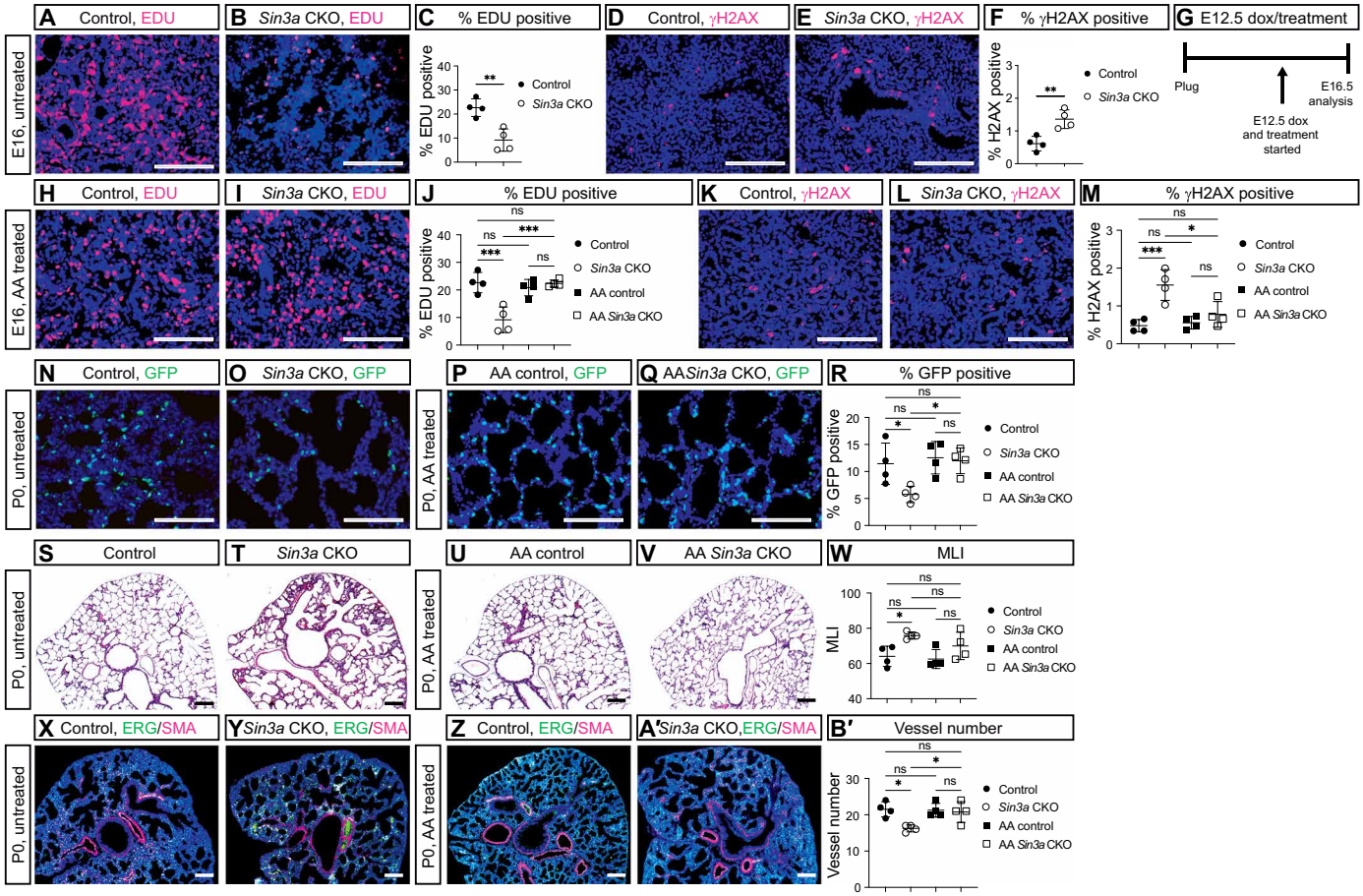

Fig. 8. Embryonic inhibition of HAT rescued lung mesenchyme and pulmonary vascular defects in *Sin3a* CKO mice. (**A** and **B**) Images of EDU (magenta) immunofluorescence in untreated E16 control (A) and *Sin3a* CKO (B) lungs. (**C**) Graph comparing the percentage of EDU-positive cells in untreated E16 control and *Sin3a* CKO lungs (**$P = 0.004$). (**D** and **E**) Images of γH2AX (magenta) immunofluorescence in untreated E16 control (D) and *Sin3a* CKO (E) lungs. (**F**) Graph comparing the percentage of γH2AX-positive cells in untreated E16 control and *Sin3a* CKO lungs (**$P = 0.007$). (**G**) Schematic of embryonic treatment regimen used in subsequent experiments starting when doxycycline is given to induce recombination at E12. (**H** and **I**) Images of EDU immunofluorescence in anacardic acid (AA)–treated E16 control (H) and *Sin3a* CKO (I) lungs. (**J**) Graph comparing the percentage of EDU-positive cells in untreated and AA-treated E16 control and *Sin3a* CKO lungs (untreated control versus AA-treated control, $P = 0.87$; untreated *Sin3a* CKO versus AA-treated *Sin3a* CKO, ***$P = 0.0007$; untreated control versus AA-treated *Sin3a* CKO, $P > 0.99$). (**K** and **L**) Images of γH2AX immunofluorescence in AA-treated E16 control (K) and *Sin3a* CKO (L) lungs. (**M**) Graph comparing the percentage of γH2AX-positive cells in untreated and AA-treated E16 control and *Sin3a* CKO lungs (untreated control versus AA-treated control, $P = 0.99$; untreated *Sin3a* CKO versus AA-treated *Sin3a* CKO, *$P = 0.01$; untreated control versus AA-treated *Sin3a* CKO, $P = 0.48$). (**N** to **Q**) Images of *Pdgfrα*-GFP immunofluorescence (GFP, green) in E16 untreated control (N) and *Sin3a* CKO (O) and AA-treated control (P) and *Sin3a* CKO (Q) lungs. (**R**) Graph comparing the percentage of GFP-positive cells in untreated and AA-treated E16 control and *Sin3a* CKO lungs (untreated control versus AA-treated control, $P = 0.94$; untreated *Sin3a* CKO versus AA-treated *Sin3a* CKO, *$P = 0.04$; untreated control versus AA-treated *Sin3a* CKO, $P = 0.99$). (**S** to **V**) Histological sections of E16 untreated control (S) and *Sin3a* CKO (T) lungs and AA-treated control (U) and *Sin3a* CKO (V) lungs. (**W**) Graph comparing the MLI of untreated and AA-treated E16 control and *Sin3a* CKO lungs (untreated control versus AA-treated control, $P = 0.98$; untreated *Sin3a* CKO versus AA-treated *Sin3a* CKO, $P = 0.47$; untreated control versus AA-treated *Sin3a* CKO, $P = 0.47$). (**X** to **A′**) Images of ERG (green) and SMA (magenta) immunofluorescence in E16 untreated control (X) and *Sin3a* CKO (Y) and AA-treated control (Z) and *Sin3a* CKO (A′) lungs. (**B′**) Graph comparing the number of vessels in untreated and AA-treated E16 control and AA-treated *Sin3a* CKO lungs (untreated control versus AA-treated control, $P > 0.99$; untreated *Sin3a* CKO versus AA-treated *Sin3a* CKO, *$P = 0.04$; untreated control versus AA-treated *Sin3a* CKO, $P = 0.95$). Statistical comparisons between untreated control and *Sin3a* CKO mice (C and F) were performed using unpaired *t* test. Statistical comparisons between untreated and treated control and *Sin3a* CKO mice (J, M, R, W, and B′) were made using one-way ANOVA with Tukey's test for multiple comparisons. Statistical significance was determined when the *P* value was <0.05. Scale bars, 100 μm.

Inhibition of HAT restores the balance of histone acetylation in *Sin3a* CKO mice

To determine whether the balance of histone acetylation and deacetylation could be restored despite the absence of SIN3A, control and *Sin3a* CKO embryos were treated with A-485, a potent and specific inhibitor of HAT p300/CPB (*95*), beginning at E12 (fig. S14, M to R). Treatment with A-485 resulted in decreased G_1 phase–to–S phase transition in control lungs (fig. S14, M and O) and did not change G_1 phase–to–S phase transition in *Sin3a* CKO lungs (fig. S14, N and O) compared to those that were untreated (Fig. 8, A to C). In contrast, compared to untreated control and mutant lungs (Fig. 8, D to F), DNA damage was unchanged in control lungs and decreased in *Sin3a* CKO lungs treated with A-485 (fig. S14, P to R). These data suggested that potent inhibition of p300/CBP HAT by A-485 could

make DNA resistant to damage but not accessible for replication during lung development and further supported the idea that SIN3A plays an important role in regulating the balance of histone acetylation and deacetylation.

We hypothesized that partial inhibition of acetyltransferase might restore the balance of histone acetylation necessary for DNA replication and cell proliferation and reduce DNA damage. To investigate this hypothesis, anacardic acid (AA), a naturally occurring HAT inhibitor that is 1000 times less potent than A-485 (*93*, *95*, *96*), was used to treat control and *Sin3a* CKO embryos following the regimen conducted with TSA and A-485 (Fig. 8, H to M). Compared to the amount of histone acetylation that was observed in untreated control and *Sin3a* CKO lungs (fig. S13, A to F), embryonic treatment with AA did not change histone acetylation in control lungs and reduced histone acetylation in *Sin3a* CKO lungs (fig. S15, A to F). Using the same embryonic treatment with AA, there was no difference in the number of EDU-positive cells or in the number of cells with evidence of DNA damage in control lungs treated with AA (Fig. 8, H, J, K, and M). In contrast, the number of EDU-positive cells was increased, whereas the number of cells with evidence of DNA damage was decreased in *Sin3a* CKO lungs treated with AA (Fig. 8, I, J, L and M).

To determine whether the increased cell proliferation and decreased DNA damage observed in *Sin3a* CKO embryos after AA treatment were due to inhibition of p300-CBP specifically, we treated control and *Sin3a* CKO embryos beginning at E12 with diluted A-485 to mimic the potency of AA HAT inhibition. We found that both 1:100 and 1:1000 dilutions of A-485 were sufficient to increase cell proliferation and decrease DNA damage in *Sin3a* CKO embryos (fig. S16, A to L). These data suggested that partial inhibition of HAT with either AA or A485 was sufficient to restore the balance of histone acetylation despite the loss of SIN3A. This conclusion was further supported by the finding that AA treatment resulted in an increased number of *Pdgfrα*-GFP–positive myofibroblast precursor cells in *Sin3a* CKO lungs compared with controls and untreated *Sin3a* CKO lungs (Fig. 8, N to R), reduced apoptosis (fig. S17, A to F), improved saccular development of the *Sin3a* CKO lungs (Fig. 8, S to W), and increased lung vessel number (Fig. 8, X to B′). In addition, although there was no change in body weight after treatment with AA (fig. S18A), pulmonary vascular physiological function was improved in *Sin3a* CKO mice treated with AA with reduced right ventricular hypertrophy (Fulton's index, fig. S18B) and reduced pulmonary vascular resistance (RVSP, fig. S18C).

These data support the idea that epigenetic regulation of gene expression is controlled by a balance of histone acetylation and deacetylation during embryonic development (fig. S19). Loss of this balance either by genetic deletion of a critical cofactor, such as SIN3A, or by pharmacological inhibition of HAT or HDAC may result in impaired cell cycling, DNA damage, and impaired cellular differentiation that can be restored through partial inhibition of HAT activity.

DISCUSSION

Regulation of histone acetylation is required to direct the rapid changes in gene expression and DNA replication necessary during development (*97*–*102*). The complementary activity of HAT and HDAC enzymes maintains the balance of histone acetylation and therefore controls transcriptional activation or repression as well as DNA replication (*99*, *102*). The balance of HAT and HDAC activity itself is necessary for development (*48*, *103*, *104*); however, how failure to maintain this balance contributes to congenital malformations is not clear. Here, we showed that loss of SIN3A function in the developing diaphragm and lungs caused failure of diaphragm formation and lung defects similar to those observed in patients with CDH. In the developing lungs, SIN3A was required to maintain the balance of histone acetylation, whereas loss of SIN3A resulted in defects in lung development and pulmonary hypertension, the two major contributors to mortality in patients with CDH.

The SIN3-HDAC complex is one of many chromatin modifiers that regulate gene expression and DNA replication by controlling the open or compact state of chromatin and thus access of transcription or replication factors to DNA (*53*, *105*). During development, chromatin modifications themselves are affected by changes in the environment, including exposures to toxins and changes in the mother's health, and translate these changes to the developing embryo (*106*). These interactions are especially important in human structural malformations where there is an overlapping impact of pathogenic gene variants and environmental mechanisms that contribute to the underlying defects in development (*107*–*110*).

Despite research demonstrating that epigenetic regulation of gene expression is essential for mammalian development (*20*, *21*, *23*), how loss of epigenetic regulation in humans contributes to structural malformations remains unclear. Mutations in genes that encode chromatin modifiers have been reported in patients with neurodevelopmental diseases and in diseases that occur later in life (*25*, *26*, *111*–*115*). Furthermore, defects in epigenetic gene regulation have been implicated in congenital heart disease and neural tube defects (*22*, *27*–*30*); however, mutations in genes that encode chromatin modifiers are uncommon among the genes identified in whole-exome or whole-genome sequencing in patients with structural malformations (*116*). This may be because epigenetic regulation is ubiquitously necessary during development, and disruption of these mechanisms, including loss of a critical co-factor, does not permit embryonic development.

The genetic or epigenetic mechanisms responsible for the difference in phenotypes between patients with Witteveen-Kolk syndrome and the patients in this study are unclear. Identification of *Lon peptidase 1*, *mitochondrial* (*LONP1*) sequence variants in patients with CDH and in patients with cerebral, ocular, dental, auricular, and skeletal syndrome demonstrates that subtle differences in the variants themselves can have a profound impact on the patient phenotype (*13*, *117*). The generation of modeling approaches that incorporate sequence and chromosomal structural variation and the potential functional consequences of these variants will be essential to accurately predict disease phenotype and penetrance as well as to understand more subtle changes that affect disease severity.

In the developing lung epithelium, SIN3A was shown to be required for cell cycling and branching morphogenesis (*76*). Abnormalities in lung branching have been reported in patients with CDH (*118*–*120*); however, the more common phenotypes associated with CDH include pulmonary hypertension and lung hypoplasia (*119*, *121*–*123*). SIN3A has been associated with regulation of cell cycling, and loss of SIN3A has been demonstrated to result in activation of p53, making senescence a likely subsequent loss-of-function phenotype (*59*, *124*). In adult type II alveolar epithelial cells, loss of SIN3A resulted in p53-dependent activation of senescence and fibrosis (*77*). Although senescence is a likely downstream phenotype after

the loss of SIN3A, our data suggest that the underlying mechanism responsible for this phenotype is loss of SIN3-HDAC regulation of gene expression.

Identifying fetal interventions that improve the outcome of patients with structural malformations is a major objective, especially for CDH (*125*–*129*). Although genomic analysis, including fetal exome or genome sequencing, could be a useful method to identify patients likely to respond to fetal interventions, CDH-associated sequence and copy number variants continue to be identified, and therefore, at this time, exome and whole-genome sequencing are more likely to yield a genetic diagnosis than a CDH-specific gene panel. Furthermore, although gene damaging variants have been reported more frequently in patients with complex CDH (*11*, *130*), patients with isolated CDH also have a significant burden of likely pathogenic genomic variants (*13*, *131*). Our hope is that with an increasing number of patients with CDH undergoing genomic analysis, we will be able to establish a pattern of gene variants and associated molecular pathway defects that are common in patients with both complex and isolated forms of the disease.

Making a genetic diagnosis in patients with CDH and determining which genetic variants only affect diaphragm development would help to identify patients more likely to respond to fetal surgical interventions because the lung and pulmonary vascular defects in these patients are more likely to be due to mechanical compression alone. In contrast, determining which genetic variants play a direct role in lung or pulmonary vascular development, as demonstrated in the case of *SIN3A*, could help to identify patients who may be less likely to respond to a treatment focused on mechanical compression alone. These patients are more likely to have primary defects in lung and pulmonary vascular development and are more likely to have lung hypoplasia and pulmonary hypertension that is not responsive to conventional treatment.

In addition to its role in embryonic lung development, SIN3A was recently implicated in the molecular mechanisms responsible for pulmonary hypertension by epigenetic regulation of *BMPR2* expression (*90*). In this case, intratracheal SIN3A protein administration in rats with experimentally induced pulmonary hypertension restored *Bmpr2* expression and decreased pulmonary artery pressure (*90*). This work demonstrates the role of SIN3A in adult patients and experimental models of pulmonary hypertension and complements our findings that loss of SIN3A resulted in developmental defects in lung and pulmonary vascular development as well as pulmonary hypertension, the major cause of mortality in patients with CDH.

We acknowledge important limitations of our study, including the fact that CDH is a genetically heterogeneous disease with multiple gene variants playing a role and that the mechanisms of abnormal lung and pulmonary vascular development were investigated in a mouse model of CDH. To address these limitations and build on the results related to *SIN3A* loss of function, we propose future studies to investigate the role of other genomic variants identified in patients with CDH during diaphragm, lung, and pulmonary vascular development. Our hypothesis is that patients with genomic variants that play a direct role in lung and pulmonary vascular development have more severe lung hypoplasia and pulmonary hypertension than patients with genomic variants that only affect diaphragm development. Furthermore, we propose that although CDH is a genetically and phenotypically heterogeneous disease, there may be common pathways that are differentially affected by the genome variants in patients with CDH. Identifying these common molecular pathways will help to subcategorize patients and determine which groups of patients are more or less likely to respond to high-risk fetal interventions including fetal endoluminal tracheal occlusion (FETO), fetal drug and small-molecule inhibitor treatments, and stem cell–based strategies. Last, developing approaches that alter the balance of histone acetylation and deacetylation during embryonic development may be effective for patients with SIN3A sequence variants and other genomic variants that affect the activity of HAT and HDAC enzymes. It will be important to demonstrate abnormal histone acetylation and associated changes in gene expression in lung cells from patients to determine whether loss of SIN3A causes increased histone acetylation as we observed in our mouse models of lung and pulmonary vascular defects associated with CDH. It is also essential to consider that the balance of HAT and HDAC is likely to be different in different cell populations and during different stages of development. Global inhibition of HAT enzymes might be effective at restoring normal development in one cell population while causing a pathological imbalance in neighboring populations. Therefore, developing cell-specific targeting strategies and approaches that target a narrow time during development might be necessary for this strategy to be effective and safe. Despite these limitations, we demonstrated that making a genetic diagnosis in patients with CDH enabled us to determine the underlying developmental mechanisms of abnormal diaphragm and lung formation and to identify an approach that improved lung development.

MATERIALS AND METHODS

Study design

The objective of this study was to determine the role of *Sin3a* during diaphragm and lung mesenchyme development. Our work included genomic evaluation of patients with CDH, tissue and cell lineage–specific deletion of *Sin3a* in mice during diaphragm and lung development, gross and histological analysis of *Sin3a* conditional deletion (*Sin3a* CKO) diaphragm and lung tissue, transcriptomic analysis of whole lung and recombined lung mesenchymal cells, and pulmonary vascular physiological analysis using transthoracic echocardiography and right heart catheterization in mice. *Sin3a* CKO mice and littermate controls were treated with HDAC and HAT inhibitors. Mice were selected for these experiments on the basis of their *Sin3a* CKO or control genotypes. For histological experiments, four control and four *Sin3a* CKO lung samples were used, and each histological experiment was performed at least two times. Quantification of histological images and physiological studies was conducted by blinded observers. For transcriptomic analysis of whole lungs and sorted recombined lung mesenchymal cells, four control and four *Sin3a* CKO lungs were analyzed. For sorted recombined mesenchymal single-cell transcriptomic analysis, two control and two *Sin3a* CKO lungs were used. Outliers were recorded and included.

Human genomic analysis

Blood and saliva samples from 827 patient and parent trios enrolled in the DHREAMS study were analyzed by whole-genome and -exome sequencing as described previously (*13*, *84*). Signed, informed consent was obtained from participants, and all studies were approved by the institutional review board at each participating institution and the Columbia University Irving Medical Center Institutional Review Board. Clinical data from medical records were

prospectively collected and entered in a central Research Electronic Data Capture (REDCap) database. A full description of the methods used for patient and control sequencing analysis, sequence variant confirmation, and the impact of sequence variants on gene transcript or protein structure or function was published previously (*13*, *84*).

Animal handling and genetics

Mice were housed and handled according to an animal care committee–approved protocol in a temperature-controlled environment with regular light and dark cycling, free access to food and water, and no more than five mice per cage. All experimental procedures were performed in an American Association for Accreditation of Laboratory Animal Care–accredited laboratory animal facility. All mice were bred on a mixed genetic background, and age-matched littermates were used as controls for comparison. Both male and female mice were used in all experiments.

Recombination of the *Sin3a* flox allele (*59*) was achieved by crossing with the previously described *Pax3-Cre* [the Jackson Laboratory, 005549 (*132*)], *Prx1-Cre* [the Jackson Laboratory, 005584 (*133*)], *Cdh5-Cre* [the Jackson Laboratory, 006137 (*134*)], or *Tbx4-rtTA; Tet-o-Cre* alleles (*135*). *Tbx4-rtTA* was induced by feeding pregnant mice doxycycline (Teklad) starting at E6.5 or E12.5. *Cre*-positive, *Sin3a*-heterogenous littermates were used as controls.

Statistical analysis

To determine statistical significance, unpaired, two-sided *t* tests were performed for comparison between two groups using Welch's correction, and one-way analysis of variance (ANOVA) was used for comparison between multiple groups for histology and physiology-based experiments. Statistical significance was determined by *Z* test for RNA velocity experiments and χ^2 test of distribution of single-cell clusters. Statistical significance for differential gene expression was adjusted with a Benjamin-Hochberg FDR correction at the 5% level.

Supplementary Materials

This PDF file includes:
Materials and Methods
Figs. S1 to S19
Tables S2 to S7

Other Supplementary Material for this manuscript includes the following:
Data file S1
Table S1
MDAR Reproducibility Checklist

REFERENCES AND NOTES

1. *Mortality in the United States, 2019*; 2020 https://cdc.gov/nchs/data/databriefs/db395-H.pdf.
2. J. Balayla, H. A. Abenhaim, Incidence, predictors and outcomes of congenital diaphragmatic hernia: A population-based study of 32 million births in the United States. *J. Matern. Fetal Neonatal Med.* **27**, 1438–1444 (2014).
3. M. R. McGivern, K. E. Best, J. Rankin, D. Wellesley, R. Greenlees, M. C. Addor, L. Arriola, H. de Walle, I. Barisic, J. Beres, F. Bianchi, E. Calzolari, B. Doray, E. S. Draper, E. Garne, M. Gatt, M. Haeusler, B. Khoshnood, K. Klungsoyr, A. Latos-Bielenska, M. O'Mahony, P. Braz, B. M. Donnell, C. Mullaney, V. Nelen, A. Queisser-Luft, H. Randrianaivo, A. Rissmann, C. Rounding, A. Sipek, R. Thompson, D. Tucker, W. Wertelecki, C. Martos, Epidemiology of congenital diaphragmatic hernia in Europe: A register-based study. *Arch. Dis. Child. Fetal Neonatal Ed.* **100**, F137–F144 (2015).
4. M. Paoletti, G. Raffler, M. S. Gaffi, L. Antounians, G. Lauriti, A. Zani, Prevalence and risk factors for congenital diaphragmatic hernia: A global view. *J. Pediatr. Surg.* **55**, 2297–2307 (2020).
5. H. Aly, D. Bianco-Batlles, M. A. Mohamed, T. A. Hammad, Mortality in infants with congenital diaphragmatic hernia: A study of the United States National Database. *J. Perinatol.* **30**, 553–557 (2010).
6. M. D. Politis, E. Bermejo-Sánchez, M. A. Canfield, P. Contiero, J. D. Cragan, S. Dastgiri, H. E. K. de Walle, M. L. Feldkamp, A. Nance, B. Groisman, M. Gatt, A. Benavides-Lara, P. Hurtado-Villa, K. Kallén, D. Landau, N. Lelong, J. Lopez-Camelo, L. Martinez, M. Morgan, O. M. Mutchinick, A. Pierini, A. Rissmann, A. Šípek, E. Szabova, W. Wertelecki, I. Zarante, M. K. Bakker, V. Kancherla, P. Mastroiacovo, W. N. Nembhard, International Clearinghouse of Birth Defects Surveillance and Research, Prevalence and mortality in children with congenital diaphragmatic hernia: A multicountry study. *Ann. Epidemiol.* **56**, 61–69.e3 (2021).
7. R. Ramakrishnan, J. L. Salemi, A. L. Stuart, H. Chen, K. O'Rourke, S. Obican, R. S. Kirby, Trends, correlates, and survival of infants with congenital diaphragmatic hernia and its subtypes. *Birth Defects Res.* **110**, 1107–1117 (2018).
8. J. Wynn, U. Krishnan, G. Aspelund, Y. Zhang, J. Duong, C. J. H. Stolar, E. Hahn, J. Pietsch, D. Chung, D. Moore, E. Austin, G. Mychaliska, R. Gajarski, Y.-L. Foong, E. Michelfelder, D. Potolka, B. Bucher, B. Warner, M. Grady, K. Azarow, S. E. Fletcher, S. Kutty, J. Delaney, T. Crombleholme, E. Rosenzweig, W. Chung, M. S. Arkovitz, Outcomes of congenital diaphragmatic hernia in the modern era of management. *J. Pediatr.* **163**, 114–119.e1 (2013).
9. R. B. Seabrook, T. R. Grover, N. Rintoul, M. Weems, S. Keene, B. Brozanski, R. DiGeronimo, B. Haberman, H. Hedrick, J. Gien, N. Ali, R. Chapman, J. Daniel, H. A. Harrison, Y. Johnson, N. F. M. Porta, M. Uhing, I. Zaniletti, K. Murthy, Children's Hospital Neonatal Consortium Congenital Diaphragmatic Hernia Focus Group, Treatment of pulmonary hypertension during initial hospitalization in a multicenter cohort of infants with congenital diaphragmatic hernia (CDH). *J. Perinatol.* **41**, 803–813 (2021).
10. E. L. Bogenschutz, Z. D. Fox, A. Farrell, J. Wynn, B. Moore, L. Yu, G. Aspelund, G. Marth, M. Yandell, Y. Shen, W. K. Chung, G. Kardon, Deep whole-genome sequencing of multiple proband tissues and parental blood reveals the complex genetic etiology of congenital diaphragmatic hernias. *HGG Adv.* **1**, 100008 (2020).
11. M. Longoni, F. A. High, H. Qi, M. P. Joy, R. Hila, C. M. Coletti, J. Wynn, M. Loscertales, L. Shan, C. J. Bult, J. M. Wilson, Y. Shen, W. K. Chung, P. K. Donahoe, Genome-wide enrichment of damaging de novo variants in patients with isolated and complex congenital diaphragmatic hernia. *Hum. Genet.* **136**, 679–691 (2017).
12. H. Qi, L. Yu, X. Zhou, J. Wynn, H. Zhao, Y. Guo, N. Zhu, A. Kitaygorodsky, R. Hernan, G. Aspelund, F.-Y. Lim, T. Crombleholme, R. Cusick, K. Azarow, M. E. Danko, D. Chung, B. W. Warner, G. B. Mychaliska, D. Potoka, A. J. Wagner, M. E. Fiky, J. M. Wilson, D. Nickerson, M. Bamshad, F. A. High, M. Longoni, P. K. Donahoe, W. K. Chung, Y. Shen, De novo variants in congenital diaphragmatic hernia identify MYRF as a new syndrome and reveal genetic overlaps with other developmental disorders. *PLOS Genet.* **14**, e1007822 (2018).
13. L. Qiao, L. Xu, L. Yu, J. Wynn, R. Hernan, X. Zhou, C. Farkouh-Karoleski, U. S. Krishnan, J. Khlevner, A. De, A. Zygmunt, T. Crombleholme, F. Y. Lim, H. Needelman, R. A. Cusick, G. B. Mychaliska, B. W. Warner, A. J. Wagner, M. E. Danko, D. Chung, D. Potoka, P. Kosiński, D. J. McCulley, M. Elfiky, K. Azarow, E. Fialkowski, D. Schindel, S. Z. Soffer, J. B. Lyon, J. M. Zalieckas, B. N. Vardarajan, G. Aspelund, V. P. Duron, F. A. High, X. Sun, P. K. Donahoe, Y. Shen, W. K. Chung, Rare and de novo variants in 827 congenital diaphragmatic hernia probands implicate LONP1 as candidate risk gene. *Am. J. Hum. Genet.* **108**, 1964–1980 (2021).
14. A. J. Merrell, B. J. Ellis, Z. D. Fox, J. A. Lawson, J. A. Weiss, G. Kardon, Muscle connective tissue controls development of the diaphragm and is a source of congenital diaphragmatic hernias. *Nat. Genet.* **47**, 496–504 (2015).
15. K. G. Ackerman, J. Wang, L. Luo, Y. Fujiwara, S. H. Orkin, D. R. Beier, *Gata4* is necessary for normal pulmonary lobar development. *Am. J. Respir. Cell Mol. Biol.* **36**, 391–397 (2007).
16. K. G. Ackerman, B. J. Herron, S. O. Vargas, H. Huang, S. G. Tevosian, L. Kochilas, C. Rao, B. R. Pober, R. P. Babiuk, J. A. Epstein, J. J. Greer, D. R. Beier, *Fog2* is required for normal diaphragm and lung development in mice and humans. *PLOS Genet.* **1**, 58–65 (2005).
17. M. K. Russell, M. Longoni, J. Wells, F. I. Maalouf, A. A. Tracy, M. Loscertales, K. G. Ackerman, B. R. Pober, K. Lage, C. J. Bult, P. K. Donahoe, Congenital diaphragmatic hernia candidate genes derived from embryonic transcriptomes. *Proc. Natl. Acad. Sci. U.S.A.* **109**, 2978–2983 (2012).
18. R. Carmona, A. Cañete, E. Cano, L. Ariza, A. Rojas, R. Muñoz-Chápuli, Conditional deletion of WT1 in the septum transversum mesenchyme causes congenital diaphragmatic hernia in mice. *eLife* **5**, e16009 (2016).
19. D. J. McCulley, M. D. Wienhold, E. A. Hines, T. A. Hacker, A. Rogers, R. J. Pewowaruk, R. Zewdu, N. C. Chesler, L. Selleri, X. Sun, *PBX* transcription factors drive pulmonary vascular adaptation to birth. *J. Clin. Invest.* **128**, 655–667 (2018).
20. J. Wu, J. Xu, B. Liu, G. Yao, P. Wang, Z. Lin, B. Huang, X. Wang, T. Li, S. Shi, N. Zhang, F. Duan, J. Ming, X. Zhang, W. Niu, W. Song, H. Jin, Y. Guo, S. Dai, L. Hu, L. Fang, Q. Wang, Y. Li, W. Li, J. Na, W. Xie, Y. Sun, Chromatin analysis in human early development reveals epigenetic transition during ZGA. *Nature* **557**, 256–260 (2018).

21. F. Santos, B. Hendrich, W. Reik, W. Dean, Dynamic reprogramming of DNA methylation in the early mouse embryo. *Dev. Biol.* **241**, 172–182 (2002).
22. R. Gilsbach, M. Schwaderer, S. Preissl, B. A. Grüning, D. Kranzhöfer, P. Schneider, T. G. Nührenberg, S. Mulero-Navarro, D. Weichenhan, C. Braun, M. Dreßen, A. R. Jacobs, H. Lahm, T. Doenst, R. Backofen, M. Krane, B. D. Gelb, L. Hein, Distinct epigenetic programs regulate cardiac myocyte development and disease in the human heart in vivo. *Nat. Commun.* **9**, 391 (2018).
23. Y. Wang, P. Yuan, Z. Yan, M. Yang, Y. Huo, Y. Nie, X. Zhu, J. Qiao, L. Yan, Single-cell multiomics sequencing reveals the functional regulatory landscape of early embryos. *Nat. Commun.* **12**, 1247 (2021).
24. E. Rexhaj, J. Bloch, P. Y. Jayet, S. F. Rimoldi, P. Dessen, C. Mathieu, J. F. Tolsa, P. Nicod, U. Scherrer, C. Sartori, Fetal programming of pulmonary vascular dysfunction in mice: Role of epigenetic mechanisms. *Am. J. Physiol. Heart Circ. Physiol.* **301**, H247–H252 (2011).
25. R. E. Amir, I. B. Van den Veyver, M. Wan, C. Q. Tran, U. Francke, H. Y. Zoghbi, Rett syndrome is caused by mutations in X-linked *MECP2*, encoding methyl-CpG-binding protein 2. *Nat. Genet.* **23**, 185–188 (1999).
26. H. Shirohzu, T. Kubota, A. Kumazawa, T. Sado, T. Chijiwa, K. Inagaki, I. Suetake, S. Tajima, K. Wakui, Y. Miki, M. Hayashi, Y. Fukushima, H. Sasaki, Three novel *DNMT3B* mutations in Japanese patients with ICF syndrome. *Am. J. Med. Genet.* **112**, 31–37 (2002).
27. N. D. E. Greene, P. Stanier, G. E. Moore, The emerging role of epigenetic mechanisms in the etiology of neural tube defects. *Epigenetics* **6**, 875–883 (2011).
28. S. Zaidi, M. Choi, H. Wakimoto, L. Ma, J. Jiang, J. D. Overton, A. Romano-Adesman, R. D. Bjornson, R. E. Breitbart, K. K. Brown, N. J. Carriero, Y. H. Cheung, J. Deanfield, S. DePalma, K. A. Fakhro, J. Glessner, H. Hakonarson, M. J. Italia, J. R. Kaltman, J. Kaski, R. Kim, J. K. Kline, T. Lee, J. Leipzig, A. Lopez, S. M. Mane, L. E. Mitchell, J. W. Newburger, M. Parfenov, I. Pe'er, G. Porter, A. E. Roberts, R. Sachidanandam, S. J. Sanders, H. S. Seiden, M. W. State, S. Subramanian, I. R. Tikhonova, W. Wang, D. Warburton, P. S. White, I. A. Williams, H. Zhao, J. G. Seidman, M. Brueckner, W. K. Chung, B. D. Gelb, E. Goldmuntz, C. E. Seidman, R. P. Lifton, De novo mutations in histone-modifying genes in congenital heart disease. *Nature* **498**, 220–223 (2013).
29. J. Cao, Q. Wu, Y. Huang, L. Wang, Z. Su, H. Ye, The role of DNA methylation in syndromic and non-syndromic congenital heart disease. *Clin. Epigenetics* **13**, 93 (2021).
30. S. Chowdhury, S. W. Erickson, S. L. MacLeod, M. A. Cleves, P. Hu, M. A. Karim, C. A. Hobbs, Maternal genome-wide DNA methylation patterns and congenital heart defects. *PLOS ONE* **6**, e16506 (2011).
31. E. Li, T. H. Bestor, R. Jaenisch, Targeted mutation of the DNA methyltransferase gene results in embryonic lethality. *Cell* **69**, 915–926 (1992).
32. M. Okano, D. W. Bell, D. A. Haber, E. Li, DNA methyltransferases Dnmt3a and Dnmt3b are essential for de novo methylation and mammalian development. *Cell* **99**, 247–257 (1999).
33. G. Lagger, D. O'Carroll, M. Rembold, H. Khier, J. Tischler, G. Weitzer, B. Schuettengruber, C. Hauser, R. Brunmeir, T. Jenuwein, C. Seiser, Essential function of histone deacetylase 1 in proliferation control and CDK inhibitor repression. *EMBO J.* **21**, 2672–2681 (2002).
34. R. L. Montgomery, C. A. Davis, M. J. Potthoff, M. Haberland, J. Fielitz, X. Qi, J. A. Hill, J. A. Richardson, E. N. Olson, Histone deacetylases 1 and 2 redundantly regulate cardiac morphogenesis, growth, and contractility. *Genes Dev.* **21**, 1790–1802 (2007).
35. Y. Wang, Y. Tian, M. P. Morley, M. M. Lu, F. J. Demayo, E. N. Olson, E. E. Morrisey, Development and regeneration of Sox2+ endoderm progenitors are regulated by a Hdac1/2-Bmp4/Rb1 regulatory pathway. *Dev. Cell* **24**, 345–358 (2013).
36. Y. Wang, D. B. Frank, M. P. Morley, S. Zhou, X. Wang, M. M. Lu, M. A. Lazar, E. E. Morrisey, HDAC3-dependent epigenetic pathway controls lung alveolar epithelial cell remodeling and spreading via miR-17-92 and TGF-β signaling regulation. *Dev. Cell* **36**, 303–315 (2016).
37. K. Ito, M. Ito, W. M. Elliott, B. Cosio, G. Caramori, O. M. Kon, A. Barczyk, S. Hayashi, I. M. Adcock, J. C. Hogg, P. J. Barnes, Decreased histone deacetylase activity in chronic obstructive pulmonary disease. *N. Engl. J. Med.* **352**, 1967–1976 (2005).
38. K. Ito, G. Caramori, S. Lim, T. Oates, K. F. Chung, P. J. Barnes, I. M. Adcock, Expression and activity of histone deacetylases in human asthmatic airways. *Am. J. Respir. Crit. Care Med.* **166**, 392–396 (2002).
39. B. G. Cosío, B. Mann, K. Ito, E. Jazrawi, P. J. Barnes, K. F. Chung, I. M. Adcock, Histone acetylase and deacetylase activity in alveolar macrophages and blood mononocytes in asthma. *Am. J. Respir. Crit. Care Med.* **170**, 141–147 (2004).
40. M. Li, Y. Zheng, H. Yuan, Y. Liu, X. Wen, Effects of dynamic changes in histone acetylation and deacetylase activity on pulmonary fibrosis. *Int. Immunopharmacol.* **52**, 272–280 (2017).
41. C. M. Robinson, R. Neary, A. Levendale, C. J. Watson, J. A. Baugh, Hypoxia-induced DNA hypermethylation in human pulmonary fibroblasts is associated with Thy-1 promoter methylation and the development of a pro-fibrotic phenotype. *Respir. Res.* **13**, 74 (2012).
42. Y. Gan, Y. H. Shen, J. Wang, X. Wang, B. Utama, X. L. Wang, Role of histone deacetylation in cell-specific expression of endothelial nitric-oxide synthase. *J. Biol. Chem.* **280**, 16467–16475 (2005).
43. H. J. Bogaard, S. Mizuno, A. A. Al Hussaini, S. Toldo, A. Abbate, D. Kraskauskas, M. Kasper, R. Natarajan, N. F. Voelkel, Suppression of histone deacetylases worsens right ventricular dysfunction after pulmonary artery banding in rats. *Am. J. Respir. Crit. Care Med.* **183**, 1402–1410 (2011).
44. A. Ruiz-Carrillo, L. J. Wangh, V. G. Allfrey, Processing of newly synthesized histone molecules. *Science* **190**, 117–128 (1975).
45. A. T. Annunziato, R. L. Seale, Histone deacetylation is required for the maturation of newly replicated chromatin. *J. Biol. Chem.* **258**, 12675–12684 (1983).
46. M. H. Kuo, C. D. Allis, Roles of histone acetyltransferases and deacetylases in gene regulation. *Bioessays* **20**, 615–626 (1998).
47. J.-H. Lee, S. R. L. Hart, D. G. Skalnik, Histone deacetylase activity is required for embryonic stem cell differentiation. *Genesis* **38**, 32–38 (2004).
48. M. Haberland, R. L. Montgomery, E. N. Olson, The many roles of histone deacetylases in development and physiology: Implications for disease and therapy. *Nat. Rev. Genet.* **10**, 32–42 (2009).
49. B. T. Weinert, T. Narita, S. Satpathy, B. Srinivasan, B. K. Hansen, C. Schölz, W. B. Hamilton, B. E. Zucconi, W. W. Wang, W. R. Liu, J. M. Brickman, E. A. Kesicki, A. Lai, K. D. Bromberg, P. A. Cole, C. Choudhary, Time-resolved analysis reveals rapid dynamics and broad scope of the CBP/p300 acetylome. *Cell* **174**, 231–244.e12 (2018).
50. R. D. W. Kelly, S. M. Cowley, The physiological roles of histone deacetylase (HDAC) 1 and 2: Complex co-stars with multiple leading parts. *Biochem. Soc. Trans.* **41**, 741–749 (2013).
51. M. Bantscheff, C. Hopf, M. M. Savitski, A. Dittmann, P. Grandi, A. M. Michon, J. Schlegl, Y. Abraham, I. Becher, G. Bergamini, M. Boesche, M. Delling, B. Dümpelfeld, D. Eberhard, C. Huthmacher, T. Mathieson, D. Poeckel, V. Reader, K. Strunk, G. Sweetman, U. Kruse, G. Neubauer, N. G. Ramsden, G. Drewes, Chemoproteomics profiling of HDAC inhibitors reveals selective targeting of HDAC complexes. *Nat. Biotechnol.* **29**, 255–265 (2011).
52. Y. Zhang, H. H. Ng, H. Erdjument-Bromage, P. Tempst, A. Bird, D. Reinberg, Analysis of the NuRD subunits reveals a histone deacetylase core complex and a connection with DNA methylation. *Genes Dev.* **13**, 1924–1935 (1999).
53. G. E. Adams, A. Chandru, S. M. Cowley, Co-repressor, co-activator and general transcription factor: The many faces of the Sin3 histone deacetylase (HDAC) complex. *Biochem. J.* **475**, 3921–3932 (2018).
54. C. A. Hassig, T. C. Fleischer, A. N. Billin, S. L. Schreiber, D. E. Ayer, Histone deacetylase activity is required for full transcriptional repression by mSin3A. *Cell* **89**, 341–347 (1997).
55. C. D. Laherty, W.-M. Yang, J.-M. Sun, J. R. Davie, E. Seto, R. N. Eisenman, Histone deacetylases associated with the mSin3 corepressor mediate mad transcriptional repression. *Cell* **89**, 349–356 (1997).
56. L. Nagy, H. Y. Kao, D. Chakravarti, R. J. Lin, C. A. Hassig, D. E. Ayer, S. L. Schreiber, R. M. Evans, Nuclear receptor repression mediated by a complex containing SMRT, mSin3A, and histone deacetylase. *Cell* **89**, 373–380 (1997).
57. D. Kadosh, K. Struhl, Repression by Ume6 involves recruitment of a complex containing Sin3 corepressor and Rpd3 histone deacetylase to target promoters. *Cell* **89**, 365–371 (1997).
58. Y. Zhang, R. Iratni, H. Erdjument-Bromage, P. Tempst, D. Reinberg, Histone deacetylases and SAP18, a novel polypeptide, are components of a human Sin3 complex. *Cell* **89**, 357–364 (1997).
59. J.-H. Dannenberg, G. David, S. Zhong, J. van der Torre, W. H. Wong, R. A. Depinho, mSin3A corepressor regulates diverse transcriptional networks governing normal and neoplastic growth and survival. *Genes Dev.* **19**, 1581–1595 (2005).
60. L. A. Pile, E. M. Schlag, D. A. Wassarman, The SIN3/RPD3 deacetylase complex is essential for G_2 phase cell cycle progression and regulation of SMRTER corepressor levels. *Mol. Cell. Biol.* **22**, 4965–4976 (2002).
61. H. Yoshimoto, M. Ohmae, I. Yamashita, The *Saccharomyces cerevisiae GAM2/SIN3* protein plays a role in both activation and repression of transcription. *Mol. Gen. Genet.* **233**, 327–330 (1992).
62. M. Vidal, R. Strich, R. E. Esposito, R. F. Gaber, RPD1 (SIN3/UME4) is required for maximal activation and repression of diverse yeast genes. *Mol. Cell. Biol.* **11**, 6306–6316 (1991).
63. T. K. Das, J. Sangodkar, N. Negre, G. Narla, R. L. Cagan, Sin3a acts through a multi-gene module to regulate invasion in *Drosophila* and human tumors. *Oncogene* **32**, 3184–3197 (2013).
64. G. A. Baltus, M. P. Kowalski, A. V. Tutter, S. Kadam, A positive regulatory role for the mSin3A-HDAC complex in pluripotency through *Nanog* and Sox2. *J. Biol. Chem.* **284**, 6998–7006 (2009).
65. L. Icardi, R. Mori, V. Gesellchen, S. Eyckerman, L. De Cauwer, J. Verhelst, K. Vercauteren, X. Saelens, P. Meuleman, G. Leroux-Roels, K. De Bosscher, M. Boutros, J. Tavernier, The Sin3a repressor complex is a master regulator of STAT transcriptional activity. *Proc. Natl. Acad. Sci. U.S.A.* **109**, 12058–12063 (2012).
66. B. E. Bernstein, J. K. Tong, S. L. Schreiber, Genomewide studies of histone deacetylase function in yeast. *Proc. Natl. Acad. Sci. U.S.A.* **97**, 13708–13713 (2000).
67. C. A. S. Banks, Y. Zhang, S. Miah, Y. Hao, M. K. Adams, Z. Wen, J. L. Thornton, L. Florens, M. P. Washburn, Integrative modeling of a Sin3/HDAC complex sub-structure. *Cell Rep.* **31**, 107516 (2020).

68. T. P. Neufeld, A. H. Tang, G. M. Rubin, A genetic screen to identify components of the sina signaling pathway in *Drosophila* eye development. *Genetics* **148**, 277–286 (1998).
69. L. A. Pile, D. A. Wassarman, Chromosomal localization links the SIN3-RPD3 complex to the regulation of chromatin condensation, histone acetylation and gene expression. *EMBO J.* **19**, 6131–6140 (2000).
70. V. Sharma, A. Swaminathan, R. Bao, L. A. Pile, *Drosophila* SIN3 is required at multiple stages of development. *Dev. Dyn.* **237**, 3040–3050 (2008).
71. G. Pennetta, D. Pauli, The *Drosophila* Sin3 gene encodes a widely distributed transcription factor essential for embryonic viability. *Dev. Genes Evol.* **208**, 531–536 (1998).
72. A. Swaminathan, L. A. Pile, Regulation of cell proliferation and wing development by *Drosophila* SIN3 and String. *Mech. Dev.* **127**, 96–106 (2010).
73. S. M. Cowley, B. M. Iritani, S. M. Mendrysa, T. Xu, P. F. Cheng, J. Yada, H. D. Liggitt, R. N. Eisenman, The *mSin3A* chromatin-modifying complex is essential for embryogenesis and T-cell development. *Mol. Cell. Biol.* **25**, 6990–7004 (2005).
74. G. David, K. B. Grandinetti, P. M. Finnerty, N. Simpson, G. C. Chu, R. A. Depinho, Specific requirement of the chromatin modifier mSin3B in cell cycle exit and cellular differentiation. *Proc. Natl. Acad. Sci. U.S.A.* **105**, 4168–4172 (2008).
75. C. van Oevelen, C. Bowman, J. Pellegrino, P. Asp, J. Cheng, F. Parisi, M. Micsinai, Y. Kluger, A. Chu, A. Blais, G. David, B. D. Dynlacht, The mammalian Sin3 proteins are required for muscle development and sarcomere specification. *Mol. Cell. Biol.* **30**, 5686–5697 (2010).
76. C. Yao, G. Carraro, B. Konda, X. Guan, T. Mizuno, N. Chiba, M. Kostelny, A. Kurkciyan, G. David, J. L. McQualter, B. R. Stripp, Sin3a regulates epithelial progenitor cell fate during lung development. *Development* **144**, 2618–2628 (2017).
77. C. Yao, X. Guan, G. Carraro, T. Parimon, X. Liu, G. Huang, A. Mulay, H. J. Soukiasian, G. David, S. S. Weigt, J. A. Belperio, P. Chen, D. Jiang, P. W. Noble, B. R. Stripp, Senescence of alveolar type 2 cells drives progressive pulmonary fibrosis. *Am. J. Respir. Crit. Care Med.* **203**, 707–717 (2021).
78. H. C. Mefford, J. A. Rosenfeld, N. Shur, A. M. Slavotinek, V. A. Cox, R. C. Hennekam, H. V. Firth, L. Willatt, P. Wheeler, E. M. Morrow, J. Cook, R. Sullivan, A. Oh, M. T. McDonald, J. Zonana, K. Keller, M. C. Hannibal, S. Ball, J. Kussmann, J. Gorski, S. Zelewski, V. Banks, W. Smith, R. Smith, L. Paull, K. N. Rosenbaum, D. J. Amor, J. Silva, A. Lamb, E. E. Eichler, Further clinical and molecular delineation of the 15q24 microdeletion syndrome. *J. Med. Genet.* **49**, 110–118 (2012).
79. Y. Narumi-Kishimoto, N. Araki, O. Migita, T. Kawai, K. Okamura, K. Nakabayashi, T. Kaname, Y. Ozawa, H. Ozawa, F. Takada, K. Hata, Novel *SIN3A* mutation identified in a Japanese patient with Witteveen-Kolk syndrome. *Eur. J. Med. Genet.* **62**, 103547 (2019).
80. J. S. Witteveen, M. H. Willemsen, T. C. D. Dombroski, N. H. M. van Bakel, W. M. Nillesen, J. A. van Hulten, E. J. R. Jansen, D. Verkaik, H. E. Veenstra-Knol, C. M. A. van Ravenswaaij-Arts, J. S. K. Wassink-Ruiter, M. Vincent, A. David, C. Le Caignec, J. Schieving, C. Gilissen, N. Foulds, P. Rump, T. Strom, K. Cremer, A. M. Zink, H. Engels, S. A. de Munnik, J. E. Visser, H. G. Brunner, G. J. M. Martens, R. Pfundt, T. Kleefstra, S. M. Kolk, Haploinsufficiency of MeCP2-interacting transcriptional co-repressor *SIN3A* causes mild intellectual disability by affecting the development of cortical integrity. *Nat. Genet.* **48**, 877–887 (2016).
81. L. C. M. van Dongen, E. Wingbermühle, A. J. M. Dingemans, A. G. Bos-Roubos, K. Vermeulen, M. Pop-Purceleanu, T. Kleefstra, J. I. M. Egger, Behavior and cognitive functioning in Witteveen-Kolk syndrome. *Am. J. Med. Genet. A* **182**, 2384–2390 (2020).
82. X. Latypova, M. Vincent, A. Mollé, O. A. Adebambo, C. Fourgeux, T. N. Khan, A. Caro, M. Rosello, C. Orellana, D. Niyazov, D. Lederer, M. Deprez, Y. Capri, P. Kannu, A. C. Tabet, J. Levy, E. Aten, N. den Hollander, M. Splitt, J. Walia, L. L. Immken, P. Stankiewicz, K. M. Walter, S. Suchy, R. J. Louie, S. Bell, R. E. Stevenson, J. Rousseau, C. Willem, C. Retiere, X.-J. Yang, P. M. Campeau, F. Martinez, J. A. Rosenfeld, C. L. Caignec, S. Küry, S. Mercier, K. Moradkhani, S. Conrad, T. Besnard, B. Cogné, N. Katsanis, S. Bézieau, J. Poschmann, E. E. Davis, B. Isidor, Haploinsufficiency of the Sin3/HDAC corepressor complex member *SIN3B* causes a syndromic intellectual disability/autism spectrum disorder. *Am. J. Hum. Genet.* **108**, 929–941 (2021).
83. M. Balasubramanian, A. J. M. Dingemans, S. Albaba, R. Richardson, T. M. Yates, H. Cox, S. Douzgou, R. Armstrong, F. H. Sansbury, K. B. Burke, A. E. Fry, N. Ragge, S. Sharif, A. Foster, A. De Sandre-Giovannoli, S. Elouej, P. Vasudevan, S. Mansour, K. Wilson, H. Stewart, S. Heide, C. Nava, B. Keren, S. Demirdas, A. S. Brooks, M. Vincent, B. Isidor, S. Küry, M. Schouten, E. Leenders, W. K. Chung, A. van Haeringen, T. Scheffner, F.-G. Debray, S. M. White, M. I. Valenzuela Palafoll, R. Pfundt, R. Newbury-Ecob, T. Kleefstra, Comprehensive study of 28 individuals with *SIN3A*-related disorder underscoring the associated mild cognitive and distinctive facial phenotype. *Eur. J. Hum. Genet.* **29**, 625–636 (2021).
84. L. Yu, J. Wynn, L. Ma, S. Guha, G. B. Mychaliska, T. M. Crombleholme, K. S. Azarow, F. Y. Lim, D. H. Chung, D. Potoka, B. W. Warner, B. Bucher, C. A. LeDuc, K. Costa, C. Stolar, G. Aspelund, M. S. Arkovitz, W. K. Chung, De novo copy number variants are associated with congenital diaphragmatic hernia. *J. Med. Genet.* **49**, 650–659 (2012).
85. M. Tiana, B. Acosta-Iborra, L. Puente-Santamaría, P. Hernansanz-Agustin, R. Worsley-Hunt, N. Masson, F. García-Rio, D. Mole, P. Ratcliffe, W. W. Wasserman, B. Jimenez, L. Del Peso, The SIN3A histone deacetylase complex is required for a complete transcriptional response to hypoxia. *Nucleic Acids Res.* **46**, 120–133 (2018).
86. P. McDonel, J. Demmers, D. W. M. Tan, F. Watt, B. D. Hendrich, Sin3a is essential for the genome integrity and viability of pluripotent cells. *Dev. Biol.* **363**, 62–73 (2012).
87. X. Liu, S. C. Rowan, J. Liang, C. Yao, G. Huang, N. Deng, T. Xie, D. Wu, Y. Wang, A. Burman, T. Parimon, Z. Borok, P. Chen, W. C. Parks, C. M. Hogaboam, S. S. Weigt, J. Belperio, B. R. Stripp, P. W. Noble, D. Jiang, Categorization of lung mesenchymal cells in development and fibrosis. *iScience* **24**, 102551 (2021).
88. V. Bergen, M. Lange, S. Peidli, F. A. Wolf, F. J. Theis, Generalizing RNA velocity to transient cell states through dynamical modeling. *Nat. Biotechnol.* **38**, 1408–1414 (2020).
89. J. Coenen-van der Spek, R. Relator, J. Kerkhof, H. McConkey, M. A. Levy, M. L. Tedder, R. J. Louie, R. S. Fletcher, H. W. Moore, A. Childers, E. R. Farrelly, N. L. Champaigne, M. J. Lyons, D. B. Everman, R. C. Rogers, S. A. Skinner, A. Renck, D. R. Matalon, S. K. Dills, B. Monteleone, S. Demirdas, A. J. M. Dingemans, L. D. Kaat, S. M. Kolk, R. Pfundt, P. Rump, B. Sadikovic, T. Kleefstra, K. M. Butler, DNA methylation episignature for Witteveen-Kolk syndrome due to SIN3A haploinsufficiency. *Genet. Med.* **25**, 63–75 (2023).
90. M. Bisserier, P. Mathiyalagan, S. Zhang, F. Elmastour, P. Dorfmüller, M. Humbert, G. David, S. Tarzami, T. Weber, F. Perros, Y. Sassi, S. Sahoo, L. Hadri, Regulation of the methylation and expression levels of the BMPR2 gene by SIN3a as a novel therapeutic mechanism in pulmonary arterial hypertension. *Circulation* **144**, 52–73 (2021).
91. R. Kadamb, S. Mittal, N. Bansal, H. Batra, D. Saluja, Sin3: Insight into its transcription regulatory functions. *Eur. J. Cell Biol.* **92**, 237–246 (2013).
92. A. Chaubal, L. A. Pile, Same agent, different messages: Insight into transcriptional regulation by SIN3 isoforms. *Epigenetics Chromatin* **11**, 17 (2018).
93. F. J. Dekker, T. van den Bosch, N. I. Martin, Small molecule inhibitors of histone acetyltransferases and deacetylases are potential drugs for inflammatory diseases. *Drug Discov. Today* **19**, 654–660 (2014).
94. E. Menegola, F. Di Renzo, M. L. Broccia, M. Prudenziati, S. Minucci, V. Massa, E. Giavini, Inhibition of histone deacetylase activity on specific embryonic tissues as a new mechanism for teratogenicity. *Birth Defects Res. B Dev. Reprod. Toxicol.* **74**, 392–398 (2005).
95. F. Zhou, Q. Liu, L. Zhang, Q. Zhu, S. Wang, K. Zhu, R. Deng, Y. Liu, G. Yuan, X. Wang, L. Zhou, Selective inhibition of CBP/p300 HAT by A-485 results in suppression of lipogenesis and hepatic gluconeogenesis. *Cell Death Dis.* **11**, 745 (2020).
96. C. Peng, J. Zhu, H. C. Sun, X. P. Huang, W. A. Zhao, M. Zheng, L. J. Liu, J. Tian, Inhibition of histone H3K9 acetylation by anacardic acid can correct the over-expression of *Gata4* in the hearts of fetal mice exposed to alcohol during pregnancy. *PLOS ONE* **9**, e104135 (2014).
97. L. Verdone, E. Agricola, M. Caserta, E. Di Mauro, Histone acetylation in gene regulation. *Brief. Funct. Genomic. Proteomic.* **5**, 209–221 (2006).
98. L. Verdone, M. Caserta, E. Di Mauro, Role of histone acetylation in the control of gene expression. *Biochem. Cell Biol.* **83**, 344–353 (2005).
99. K. Struhl, Histone acetylation and transcriptional regulatory mechanisms. *Genes Dev.* **12**, 599–606 (1998).
100. K. W. McCool, X. Xu, D. B. Singer, F. E. Murdoch, M. K. Fritsch, The role of histone acetylation in regulating early gene expression patterns during early embryonic stem cell differentiation. *J. Biol. Chem.* **282**, 6696–6706 (2007).
101. R. Bar-Ziv, Y. Voichek, N. Barkai, Chromatin dynamics during DNA replication. *Genome Res.* **26**, 1245–1256 (2016).
102. A. Unnikrishnan, P. R. Gafken, T. Tsukiyama, Dynamic changes in histone acetylation regulate origins of DNA replication. *Nat. Struct. Mol. Biol.* **17**, 430–437 (2010).
103. A. Peserico, C. Simone, Physical and functional HAT/HDAC interplay regulates protein acetylation balance. *J. Biomed. Biotechnol.* **2011**, 371832 (2011).
104. L. Haery, R. C. Thompson, T. D. Gilmore, Histone acetyltransferases and histone deacetylases in B- and T-cell development, physiology and malignancy. *Genes Cancer* **6**, 184–213 (2015).
105. K. A. Gelato, W. Fischle, Role of histone modifications in defining chromatin structure and function. *Biol. Chem.* **389**, 353–363 (2008).
106. L. Legoff, S. C. D'Cruz, S. Tevosian, M. Primig, F. Smagulova, Transgenerational inheritance of environmentally induced epigenetic alterations during mammalian development. *Cell* **8**, 1559 (2019).
107. R. Ramakrishnan, A. L. Stuart, J. L. Salemi, H. Chen, K. O'Rourke, R. S. Kirby, Maternal exposure to ambient cadmium levels, maternal smoking during pregnancy, and congenital diaphragmatic hernia. *Birth Defects Res.* **111**, 1399–1407 (2019).
108. K. M. Caspers, C. Oltean, P. A. Romitti, L. Sun, B. R. Pober, S. A. Rasmussen, W. Yang, C. Druschel, National Birth Defects Prevention Study, Maternal periconceptional exposure to cigarette smoking and alcohol consumption and congenital diaphragmatic hernia. *Birth Defects Res. A Clin. Mol. Teratol.* **88**, 1040–1049 (2010).
109. R. H. Finnell, C. D. Caiaffa, S.-E. Kim, Y. Lei, J. Steele, X. Cao, G. Tukeman, Y. L. Lin, R. M. Cabrera, B. J. Wlodarczyk, Gene environment interactions in the etiology of neural tube defects. *Front. Genet.* **12**, 659612 (2021).

110. T. Workalemahu, K. L. Grantz, J. Grewal, C. Zhang, G. M. B. Louis, F. Tekola-Ayele, Genetic and environmental influences on fetal growth vary during sensitive periods in pregnancy. *Sci. Rep.* **8**, 7274 (2018).
111. G. W. E. Santen, E. Aten, Y. Sun, R. Almomani, C. Gilissen, M. Nielsen, S. G. Kant, I. N. Snoeck, E. A. J. Peeters, Y. Hilhorst-Hofstee, M. W. Wessels, N. S. den Hollander, C. A. L. Ruivenkamp, G.-J. B. van Ommen, M. H. Breuning, J. T. den Dunnen, A. van Haeringen, M. Kriek, Mutations in SWI/SNF chromatin remodeling complex gene *ARID1B* cause Coffin-Siris syndrome. *Nat. Genet.* **44**, 379–380 (2012).
112. S. Timmermann, H. Lehrmann, A. Polesskaya, A. Harel-Bellan, Histone acetylation and disease. *Cell. Mol. Life Sci.* **58**, 728–736 (2001).
113. S. Ropero, M. F. Fraga, E. Ballestar, R. Hamelin, H. Yamamoto, M. Boix-Chornet, R. Caballero, M. Alaminos, F. Setien, M. F. Paz, M. Herranz, J. Palacios, D. Arango, T. F. Orntoft, L. A. Aaltonen, S. Schwartz Jr., M. Esteller, A truncating mutation of *HDAC2* in human cancers confers resistance to histone deacetylase inhibition. *Nat. Genet.* **38**, 566–569 (2006).
114. K. S. Cho, L. I. Elizondo, C. F. Boerkoel, Advances in chromatin remodeling and human disease. *Curr. Opin. Genet. Dev.* **14**, 308–315 (2004).
115. E. Brookes, Y. Shi, Diverse epigenetic mechanisms of human disease. *Annu. Rev. Genet.* **48**, 237–268 (2014).
116. S. Petrovski, V. Aggarwal, J. L. Giordano, M. Stosic, K. Wou, L. Bier, E. Spiegel, K. Brennan, N. Stong, V. Jobanputra, Z. Ren, X. Zhu, C. Mebane, O. Nahum, Q. Wang, S. Kamalakaran, C. Malone, K. Anyane-Yeboa, R. Miller, B. Levy, D. B. Goldstein, R. J. Wapner, Whole-exome sequencing in the evaluation of fetal structural anomalies: A prospective cohort study. *Lancet* **393**, 758–767 (2019).
117. K. A. Strauss, R. N. Jinks, E. G. Puffenberger, S. Venkatesh, K. Singh, I. Cheng, N. Mikita, J. Thilagavathi, J. Lee, S. Sarafianos, A. Benkert, A. Koehler, A. Zhu, V. Trovillion, M. McGlincy, T. Morlet, M. Deardorff, A. M. Innes, C. Prasad, A. E. Chudley, I. N. W. Lee, C. K. Suzuki, CODAS syndrome is associated with mutations of LONP1, encoding mitochondrial AAA+ Lon protease. *Am. J. Hum. Genet.* **96**, 121–135 (2015).
118. K. Nose, S. Kamata, T. Sawai, Y. Tazuke, N. Usui, H. Kawahara, A. Okada, Airway anomalies in patients with congenital diaphragmatic hernia. *J. Pediatr. Surg.* **35**, 1562–1565 (2000).
119. D. Ameis, N. Khoshgoo, R. Keijzer, Abnormal lung development in congenital diaphragmatic hernia. *Semin. Pediatr. Surg.* **26**, 123–128 (2017).
120. C. A. Ryan, N. N. Finer, P. C. Etches, A. J. Tierney, A. Peliowski, Congenital diaphragmatic hernia: Associated malformations—Cystic adenomatoid malformation, extralobular sequestration, and laryngotracheoesophageal cleft: Two case reports. *J. Pediatr. Surg.* **30**, 883–885 (1995).
121. D. Kluth, R. Tenbrinck, M. von Ekesparre, R. Kangah, P. Reich, A. Brandsma, D. Tibboel, W. Lambrecht, The natural history of congenital diaphragmatic hernia and pulmonary hypoplasia in the embryo. *J. Pediatr. Surg.* **28**, 456–463 (1993).
122. H. Mohseni-Bod, D. Bohn, Pulmonary hypertension in congenital diaphragmatic hernia. *Semin. Pediatr. Surg.* **16**, 126–133 (2007).
123. B. Thébaud, J. C. Mercier, A. T. Dinh-Xuan, Congenital diaphragmatic hernia. A cause of persistent pulmonary hypertension of the newborn which lacks an effective therapy. *Biol. Neonate* **74**, 323–336 (1998).
124. D. S. Wilkinson, W.-W. Tsai, M. A. Schumacher, M. C. Barton, Chromatin-bound p53 anchors activated Smads and the mSin3A corepressor to confer transforming growth factor β-mediated transcription repression. *Mol. Cell. Biol.* **28**, 1988–1998 (2008).
125. L. Antounians, V. D. Catania, L. Montalva, B. D. Liu, H. Hou, C. Chan, A. C. Matei, A. Tzanetakis, B. Li, R. L. Figueira, K. M. da Costa, A. P. Wong, R. Mitchell, A. L. David, K. Patel, P. De Coppi, L. Sbragia, M. D. Wilson, J. Rossant, A. Zani, Fetal lung underdevelopment is rescued by administration of amniotic fluid stem cell extracellular vesicles in rodents. *Sci. Transl. Med.* **13**, eaax5941 (2021).
126. F. Okolo, G. Zhang, J. Rhodes, G. K. Gittes, D. A. Potoka, Intra-amniotic sildenafil treatment promotes lung growth and attenuates vascular remodeling in an experimental model of congenital diaphragmatic hernia. *Fetal Diagn. Ther.* **47**, 787–799 (2020).
127. D. S. Mous, H. M. Kool, P. E. Burgisser, M. J. Buscop-van Kempen, K. Nagata, A. Boerema-de Munck, J. van Rosmalen, O. Dzyubachyk, R. M. H. Wijnen, D. Tibboel, R. J. Rottier, Treatment of rat congenital diaphragmatic hernia with sildenafil and NS-304, selexipag's active compound, at the pseudoglandular stage improves lung vasculature. *Am. J. Physiol. Lung Cell. Mol. Physiol.* **315**, L276–L285 (2018).
128. C. Jeanty, S. M. Kunisaki, T. C. MacKenzie, Novel non-surgical prenatal approaches to treating congenital diaphragmatic hernia. *Semin. Fetal Neonatal Med.* **19**, 349–356 (2014).
129. M. A. Verla, C. C. Style, O. O. Olutoye, Prenatal intervention for the management of congenital diaphragmatic hernia. *Pediatr. Surg. Int.* **34**, 579–587 (2018).
130. L. Yu, A. D. Sawle, J. Wynn, G. Aspelund, C. J. Stolar, M. S. Arkovitz, D. Potoka, K. S. Azarow, G. B. Mychaliska, Y. Shen, W. K. Chung, Increased burden of de novo predicted deleterious variants in complex congenital diaphragmatic hernia. *Hum. Mol. Genet.* **24**, 4764–4773 (2015).
131. E. Brosens, N. C. J. Peters, K. S. van Weelden, C. Bendixen, R. W. W. Brouwer, F. Sleutels, H. T. Bruggenwirth, W. F. J. van Ijcken, D. C. M. Veenma, S. C. M. Cochius-Den Otter, R. M. H. Wijnen, A. J. Eggink, M. F. van Dooren, H. M. Reutter, R. J. Rottier, J. M. Schnater, D. Tibboel, A. de Klein, Unraveling the genetics of congenital diaphragmatic hernia: An ongoing challenge. *Front. Pediatr.* **9**, 800915 (2021).
132. K. A. Engleka, A. D. Gitler, M. Zhang, D. D. Zhou, F. A. High, J. A. Epstein, Insertion of Cre into the *Pax3* locus creates a new allele of *Splotch* and identifies unexpected *Pax3* derivatives. *Dev. Biol.* **280**, 396–406 (2005).
133. M. Logan, J. F. Martin, A. Nagy, C. Lobe, E. N. Olson, C. J. Tabin, Expression of Cre recombinase in the developing mouse limb bud driven by a *Prxl* enhancer. *Genesis* **33**, 77–80 (2002).
134. J. A. Alva, A. C. Zovein, A. Monvoisin, T. Murphy, A. Salazar, N. L. Harvey, P. Carmeliet, M. L. Iruela-Arispe, VE-Cadherin-Cre-recombinase transgenic mouse: A tool for lineage analysis and gene deletion in endothelial cells. *Dev. Dyn.* **235**, 759–767 (2006).
135. W. Zhang, D. B. Menke, M. Jiang, H. Chen, D. Warburton, G. Turcatel, C. H. Lu, W. Xu, Y. Luo, W. Shi, Spatial-temporal targeting of lung-specific mesenchyme by a *Tbx4* enhancer. *BMC Biol.* **11**, 111 (2013).

Acknowledgments: We thank G. David (New York University Grossman School of Medicine) and W. Shi (Keck School of Medicine, University of Southern California) for sharing mouse strains; the University of Wisconsin-Madison Gene Expression Center and Bioinformatics Resource Center for help conducting and analyzing the RNA sequencing experiments; the University of Wisconsin Carbone Cancer Center FLOW Cytometry Laboratory, where lung mesenchymal cell sorting was conducted; and the University of Wisconsin-Madison Optical Imaging Core and the University of California, San Diego School of Medicine Microscopy Core, where the confocal imaging was conducted. We also thank A. Ikeda and the members of the Ikeda laboratory (University of Wisconsin-Madison) and X. Sun and members of the Sun laboratory (University of California, San Diego) for discussion and review of this manuscript. We also thank the patients and family members who have participated in the DHREAMs study. **Funding:** This work was supported by the following: Translational Science Career Development Award KL2TR000428 (D.J.M.), a subaward from the National Center for Advancing Translational Sciences (NCATS) grant to the University of Wisconsin-Madison Institute for Clinical and Translational Research UL1TR000427; National Institutes of Health grants NHLBI R01HL146859 (D.J.M.), NHLBI R01HL132366, R01HL136998, X01HL140543 (Y.S. and W.K.C.), and NICHD P01HD068250 (Y.S., W.K.C., and D.J.M.); National Key Research and Development Program of China 2019YFE0119400 (H.T.); and Natural Science Foundation of China 81770059, 81970052, and 82170057 (H.T.). **Author contributions:** Conceptualization: W.K.C. and D.J.M. Methodology: G. Stokes, J.X.-J.Y., N.C.C., Y.S., W.K.C., and D.J.M. Investigation: G. Stokes, Z.L., N.T., W.G., M.B.B., B.P., M.D.W., G. Sandok, R.H., J.W., H.T., D.M.T., A.R., T.A.H., P.Z., R.M., and D.J.M. Funding acquisition: Y.S., W.K.C., and D.J.M. Writing—original draft: G. Stokes and D.J.M. Writing—review and editing: G. Stokes, Z.L., M.B.B., B.P., N.C.C., R.M., Y.S., W.K.C., and D.J.M. **Competing interests:** The authors declare that they have no competing interests. **Data and materials availability:** All data associated with this study are present in the paper or the Supplementary Materials. All raw sequencing data and processed files have been deposited in GEO under the series reference GSE246195. Mice carrying the *Sin3a* flox allele (*59*) were shared by G. David under a material agreement with New York University Grossman School of Medicine. Mice carrying the *Tbx4-rtTA; Tet-o-Cre* alleles (*135*) were shared by W. Shi under a material agreement with Keck School of Medicine, University of Southern California.

Submitted 10 May 2022
Resubmitted 1 July 2023
Accepted 10 January 2024
Published 31 January 2024
10.1126/scitranslmed.adc8930